International Journal of Disaster Risk Reduction 135 (2026) 106040

Contents lists available at ScienceDirect

International Journal of Disaster Risk Reduction

journal homepage: www.elsevier.com/locate/ijdrr

Forecasting tephra fall building impacts and losses at Awu volcano, Sangihe Island (Indonesia)

Eleanor Tennant [a,*], Susanna F. Jenkins [b], Christina Widiwijayanti [b], Ahmad Basuki [c], Heruningtyas D. Purnamasari [c]

[a] Earth Observatory of Singapore, Interdisciplinary Graduate Programme, Nanyang Technological University, 639798, Singapore
[b] Earth Observatory of Singapore and Asian School of the Environment, Nanyang Technological University, 639798, Singapore
[c] Center for Volcanology and Geological Hazard Mitigation, Bandung city, West Java, 40122, Indonesia

A R T I C L E I N F O

Keywords:
Volcanic risk
Vulnerability
Impact forecasting
Quantitative risk assessment
Losses

A B S T R A C T

Moving beyond volcanic hazard assessment to forecast how hazards affect communities provides valuable information for risk mitigation. Awu, a remote volcano on Sangihe Besar Island, Indonesia, is currently experiencing unrest (December 2025). With the entire population living within 45 km of the volcano, there is a need for actionable risk information. We integrated probabilistic tephra fall hazard analysis with building exposure and vulnerability information to forecast losses from a likely VEI 4 eruption. To address limited exposure data, we extracted building roof types from satellite imagery and applied Bayesian inference to combine existing vulnerability models into a hybrid framework suited to local conditions. Results indicate a 95% probability of exceeding ~$11 million USD (~179 billion IDR) in building damage and a 75% probability of exceeding $25 million USD (~407 billion IDR). Losses are concentrated in the northern districts, with Tahuna, the capital most affected. Losses at Awu were not well forecast by column height and wind conditions, parameters currently used to trigger insurance payouts from volcanic catastrophe risk bonds. Existing probabilistic volcanic loss calculations often couple a single hazard footprint representing the N^{th} percentile intensity with exposure and vulnerability data. Here we calculated loss for each individual hazard footprint computing 100 million values to capture uncertainty in both hazard and vulnerability. Losses calculated using the median hazard footprint were 5% higher than the median of the loss population. In addition to supporting decision making during the current unrest, our work presents key advancements in volcanic risk assessment that may be applied to other locations worldwide.

1. Introduction

Assessing the potential consequences or impacts of an eruption before or during volcanic unrest can help to mitigate volcanic risk. These insights are often more valuable than hazard forecasts alone, as they enable better-informed decisions regarding preparedness measures such as land-use planning, construction design codes, financial risk transfer mechanisms, understanding evacuation needs, and resource allocation [1,2].

Risk assessment integrates hazard, exposure, and vulnerability information to understand the potential losses, that are often

* Corresponding author.
E-mail address: eleanorm001@e.ntu.edu.sg (E. Tennant).

https://doi.org/10.1016/j.ijdrr.2026.106040
Received 16 August 2025; Received in revised form 26 January 2026; Accepted 29 January 2026
Available online 31 January 2026

expressed in financial terms (e.g., [3]), as the number of people or assets affected (e.g., [4–8]) or through spatial risk rankings (e.g., [9–13]). Compared to other natural hazards such as earthquakes and tsunami, there are fewer cases in volcanology that go beyond hazard assessment to integrate hazard with exposure and vulnerability information. This gap is likely compounded by the lack of consensus on appropriate volcanic risk assessment methodologies [14], and by the limited availability of physical vulnerability models that link hazard intensity to expected damage [15]. For example, impacts from tephra fall are the most well documented compared to other hazards [16], yet for buildings there are currently only nine sets of published vulnerability models to describe the range of building types globally (references in [17]).

In volcanic hazard assessment, probabilistic approaches are commonly used to account for uncertainty that arises due to limited datasets and the natural variability of volcanic systems, (e.g., Ref. [18–22]). Under a probabilistic framework distributions of hazard model input parameters are built and sampled from to generate a range of possible outcomes and their likelihood of occurrence. However, characterisation of uncertainty is less common in volcanic risk assessments [23]. Past approaches have coupled a single hazard footprint – representing the N^{th} percentile hazard intensity, or the intensity associated with a certain probability – with exposure and vulnerability information (e.g., [10,13,24–26]). Efforts to incorporate uncertainty into exposure estimates have involved assigning weighted probabilities to building typologies (e.g., [27,28]). Uncertainty in the vulnerability component has typically been addressed through the use of fragility curves, which provide damage state probabilities as a function of a given hazard intensity (e.g., [15,29,30]), with some accounting for uncertainty around this curve (e.g. [31]). Alternative approaches have combined vulnerability model confidence bounds with various hazard intensity thresholds, to create an uncertainty matrix for agricultural risk from tephra fall [8]. While these studies provide important insights, to date there has been limited work that propagates uncertainty from hazard through to loss.

To address this gap we implemented a probabilistic framework to forecast the potential impacts associated with tephra fall from a VEI 4 eruption at Awu volcano, Sangihe Besar Island (referred to as Sangihe Island from hereon in) Indonesia. Advancing volcanic risk assessment is particularly crucial for Sangihe Island, where recent work has highlighted social, economic and physical vulnerability to landslides, flooding, and earthquakes [32]. We focus on tephra fall, the most widespread volcanic hazard capable of causing building damage tens of kms away from a volcano [29]. Buildings are a critical asset, providing shelter, supporting livelihoods and representing the most valuable insurable asset [33]. Forecasting the number of affected buildings, their spatial distribution, and the associated financial losses can provide valuable information to guide preparedness and, in the event of an eruption, support recovery efforts at Awu.

In this work we offer three main contributions: 1) We provide the first volcanic hazard and risk assessment for Awu volcano; drawing from approaches for other natural hazards, we systematically integrate uncertainty from hazard through to risk. 2) In absence

Fig. 1. Map showing the location of Awu volcano on Sangihe Island and (inset) within southeast Asia. Blue circles mark radial distances away from the summit. Base map: ESRI shaded relief. Building footprints: Google Open Buildings. Coordinate reference system: EPSG: 32651.

of building typology information we develop a straightforward method to derive building exposure information from satellite imagery. 3) We address limitations in the availability of suitable building vulnerability models by using Bayesian inference to combine disparate datasets.

1.1. Geographic setting and eruptive history

Awu is an active volcano, located on Sangihe Island within the Sangihe Islands regency in North Sulawesi province, Indonesia (Fig. 1). It is the northernmost of the eight active volcanoes comprising the Sangihe Arc, which extends approximately 500 km from northeastern Sulawesi up to Mindanao in the Philippines.

Awu has 18 eruptions in its historic record (378 years): 1640 *(phreatic)*, 1646 *(VEI 2)*, 1677 *(phreatic),* 1711 *(VEI 3),* 1812 *(VEI 4)*, 1856 *(VEI 3),* 1875 *(VEI 2),* 1883 *(VEI 2),* 1885 *(VEI 2),* 1892 *(VEI 3),* 1893 *(VEI 2),* 1913 *(VEI 2),* 1921 *(phreatic),* 1922 *(phreatic),* 1930 *(VEI 2),* 1966 *(VEI 4),* 1992 *(VEI 1)*, 2004 *(VEI 2)* [34,35]. Past eruptions have been short-lived, lasting between one and six days [35,36], and the majority (13 out of 18) have been phreatomagmatic or phreatic in nature [34]. Awu's summit crater has alternated between hosting a crater lake and a lava dome. Lakes were present in 1922, 1973, and 1995, while both a crater lake and a lava dome co-existed in 1931 and 1979 [34]. The most recent large ($\geq$ VEI 3) eruption was the 1966 VEI 4 eruption which occurred with little precursory activity [37] and was influenced by a 3×10^6 m^3 lava dome emplaced in 1931, that plugged the conduit and contributed to the eruption's intensity [34]. The latest eruption (2004) was a VEI 2 effusive and explosive event, that produced column heights up to 3 km above sea level (asl) and erupted a basaltic andesite lava dome with a volume of 2.8×10^6 m^3 [34].

Past eruptions at Awu have had catastrophic consequences, resulting in a total of 11,048 fatalities, mostly from PDCs and lahars during the 1711, 1812, and 1856 eruptions [34] making Awu one of the deadliest volcanoes in the world [38]. While flow hazards have been the primary cause of loss of life, tephra fall has also caused widespread damage and disruption. Tephra fall building damage was reported in Tahuna, the regency capital located 8–11 km south-southeast of the volcano following VEI 3 eruptions in 1856 and 1892 (Colonial Times Hobart, 1856; Nature, 1892). During the 1966 (VEI 4) eruption tephra fall affected the western side of Sangihe Island damaging buildings in Kendahe and Talawid villages, located 6 km and 7 km from the vent respectively [37]. Winds carried most tephra offshore to the west. In contrast, the smaller VEI 2 eruption in 2004 deposited ~1 mm of tephra in Tahuna and 1.5–2 mm in Naha and Mala villages, ~9 km to the east due to variable wind conditions during its four-day explosive phase [39].

1.1.1. Current activity

In Indonesia, the Centre for Volcanology and Geological Hazard Mitigation (CVGHM) is the national agency responsible for monitoring volcanic activity, assessing volcanic hazards, and issuing alert levels and technical recommendations for risk mitigation. In May 2022 prompted by increasing seismic activity, CVGHM raised Awu's volcanic alert level to level 3 (watch) out of 4, indicating that an eruption may occur. Inflation was observed from June 2023, accompanied by a further increase in seismicity from March 2024 [35]. As of December 2025, the crater is filled with the 2004 lava dome, raising concerns about the potential for another large explosive eruption similar to the 1966 VEI 4 event. The 2014 VEI 4 eruption of Kelud volcano (East Java) has been considered by CVGHM to serve as a more recent analogue. Like the 1966 eruption at Awu a lava dome previously plugged the conduit leading to a large explosive eruption with little precursory activity [40]. Kelud's eruption caused moderate damage to destruction of ~18,000 buildings some up to ~25 km away from the volcano [41]. A similar eruption at Awu could have Island-wide impacts. We therefore based our analysis on forecasting the potential impacts associated with a VEI 4 eruption that is analogous to the 1966 eruption of Awu and the more recent 2014 eruption of Kelud.

1.2. Sangihe Island socio-economic setting

Sangihe Island is a small and remote maritime island, covering ~740 km^2, with a population of ~140,000 people [42], all living within 45 km of the volcano. The local economy is largely natural-resource–dependent, relying on agriculture, plantations, and small-scale fisheries. Approximately 17% of the total population are aged 0–14 years, 69% are of working age (15–59 years), 65% of which are economically active, with employment concentrated in agriculture, forestry, and fisheries (30%), manufacturing (16%), wholesale and retail trade (14%), and government administration (11%) [43]. The remaining ~14% of the total population are over 60 years [43]. Around 10% of residents live below the North Sulawesi regency poverty line [43]. More than half of the workforce is self-employed limiting economic buffering capacity and increasing sensitivity to environmental and economic disruptions.

Livelihoods are dominated by primary sectors that are sensitive to environmental change. Fisheries play a central role, most vessels are small (0–3 gross tonnage), reflecting a reliance on nearshore fishing [44]. Agriculture and plantations are predominantly smallholder-based, with coconut (copra), nutmeg, and cloves as the main cash crops [44]. Volcanic ashfall can therefore affect crop production, fishing activities, water quality, and access to markets. Sangihe Island relies primarily on maritime transport, with the Port of Tahuna serving as the main logistical hub connecting the island to Bitung and Manado [45]. While a network of public ports and small jetties supports inter-island mobility. This dependence on sea transport increases sensitivity to disruptions during volcanic unrest and adverse weather that may also affect evacuation, emergency access, and post-disaster recovery.

2. Method

To quantify the potential losses from a VEI 4 sized eruption at Awu, we combined probabilistic tephra fall simulations with exposure data (building location and typology) extracted from satellite image classification and fragility functions developed by combining existing functions using Bayesian inference (Fig. 2). We conducted 10,000 hazard simulations and for each simulation extracted tephra accumulation at the centroid of each building footprint. For each building we applied three fragility functions to identify the most likely damage severity as described by the damage state (DS): DS2, DS3, DS4/5 using the damage state framework developed by Williams et al. [30] (Table 1). To account for uncertainty in the fragility functions, for each hazard simulation for each building we performed random sampling drawing 10,000 realisations across each curve and its confidence intervals. For each hazard simulation we computed the total losses across all buildings for each vulnerability sample.

To quantify financial losses, we used the proportion of the total building replacement cost attributed to each damage state DS2, DS3, and DS4/5. Our damage states are comparable to those used in Blong [46], that have associated proportional replacement cost values of 0.1, 0.4, and 0.8 respectively. For each building, we applied a total replacement cost of USD 12,000, which includes the cost of labour and construction materials for an average sized single storey residential building, but excludes damage to contents. This value was determined during a volcanic hazard workshop held in Bandung in April 2024, through consultations with CVGHM experts. The workshop included key personnel such as the Head of the Volcano Division, the Head of Monitoring for Awu Volcano, and staff experienced in volcanic crisis management and post-disaster recovery, including those with direct involvement in the Sangihe Arc islands.

Our approach produced 10,000 $\times$ 10,000 loss estimates (N = 100 million), which were used to produce 10,000 conditional loss exceedance curves for each damage state DS2, DS3, DS4/5 capturing uncertainty in both the hazard intensity and the vulnerability.

A simplification that has been applied to volcanic risk assessment in the past is the use of the Nth percentile hazard footprint to calculate the losses assuming that this represents the Nth percentile losses. However ideally losses should be calculated for each combination of sampled hazard, exposure, and vulnerability. To understand the impact of this, in addition to the full calculation of losses, we calculated the loss associated with the 50th percentile tephra accumulation using the median value of each vulnerability

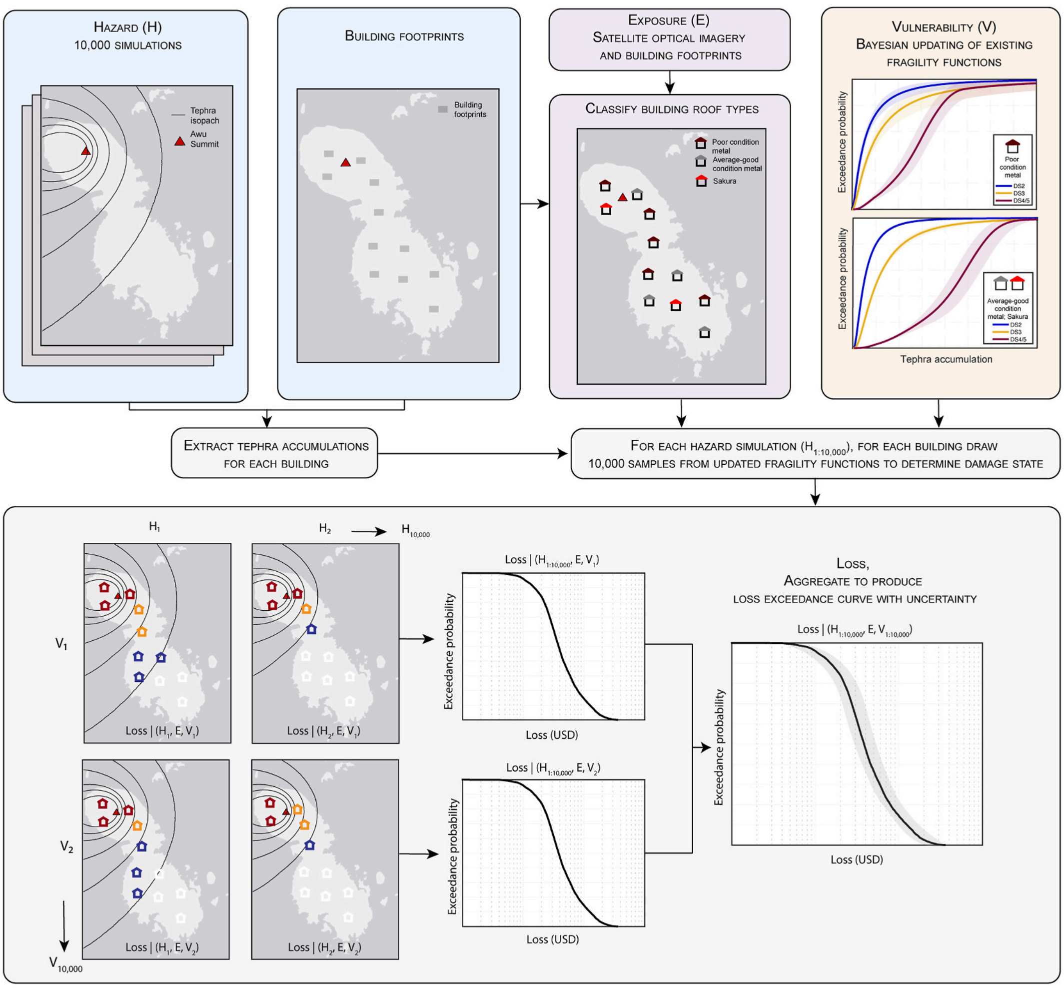

Fig. 2. Schematic overview of the study methodology. Ten thousand tephra-fall hazard simulations were combined with building exposure data derived from satellite imagery roof-type classification. For each hazard realisation, ten thousand vulnerability (V) samples were drawn from hybrid fragility functions developed using Bayesian inference. Together these produce probabilistic loss estimates.

Table 1
Tephra fall building damage states after Williams et al. [30]. Damage states were developed from remotely sensed data collected after the 2014 eruption of Kelud volcano in Indonesia.

Damage state		Description
DS2	Moderate damage	Cladding replaced for <50% of the roof area
DS3	Heavy damage	Cladding replaced for >50% of the roof area
DS4/5	Severe damage/Collapse	The roof over the central part of the building has collapsed or the building has collapsed

function for comparison.

In the sections that follow we provide more details on the quantification of the hazard, exposure and vulnerability information used in our assessment.

2.1. Tephra fall hazard

To model the spatial extent of tephra fall we used Tephra2 [47] run within the MATLAB probabilistic wrapper TephraProb [27]. Tephra2 solves the advection-diffusion equation analytically across a grid of evenly spaced points. For Awu we ran 10,000 simulations across a 100 m grid, accounting for uncertainty in the model input parameters by stochastically sampling from the ranges provided in Table 2, that were informed by the 2014 eruption of Kelud. For the plume height and erupted mass, we used the range associated with a VEI 4 sized eruption [48], using a lognormal distribution for column height to give preference to the lower values. For the particle properties, median grain size and density, we used values informed by the 2014 eruption of Kelud volcano. For the empirical Tephra2 parameters which are used to describe atmospheric diffusion (fall time threshold and the diffusion coefficient) we sampled from ranges defined by inverted field deposits from Plinian eruptions in the literature [24,49,50]. Each sampled combination of eruption source parameters (ESPs) was combined with a wind profile sampled from a 10-year range sourced from the ECMWF ERA5 atmospheric reanalysis dataset [51]. The dataset provides hourly values of atmospheric data at 37 pressure levels on a global 0.25° grid. For this work we used four profiles per day extracted at 0:00, 6:00, 12:00, 18:00. Wind roses show that throughout the year between ~10 and 18 km above sea level (asl) the dominant wind direction is towards the west (Fig. 3). At ~18 km– the approximate height of the tropopause– there is roughly equal probability of wind blowing towards the west and the east. Median wind directions per month are provided in the Supplementary material (Fig. S1) and do not show any dominant seasonal patterns.

2.2. Building exposure

The main way that tephra fall damages buildings is through collapse of the roof. Roof collapse occurs when the vertical load exceeds the capacity of the roof material, and/or supporting structure [15]. Factors that affect the vulnerability of buildings to tephra fall damage are the materials used for the roof covering and supporting structure, the age condition and construction quality, along with the roof type (e.g., gable, hip, flat) and pitch [5,29,54,55,56].

Census data for North Sulawesi province indicate that 96% of residential buildings have metal sheet roof coverings [57]. Observations made during an informal field survey on Sangihe Island in June 2025 supported this and further revealed that residential

Table 2
Tephra2 input parameter ranges used to run probabilistic simulations of a VEI 4 sized eruption at Awu volcano.

Parameter	Values
Grid	100m × 100 m
Wind data	10 years (2014–2023) ERA 5, four profiles per day
Plume height (km above vent)	10–25 km (lognormal)
Duration	1–6 h
Erupted mass	1.4×10^{11} - 1.4×10^{12} kg Calculated from the volume of a VEI 4 eruption using a bulk density of 1400 kg/m^3 [52]
Particle size bounds	-6 ϕ to 7 ϕ
Median grain size	-3-1
Standard deviation	1–3
Aggregation	30–70% of particles <63 μm [53]
Eddy constant	0.04 m^2/s
Diffusion coefficient	100-6000 (uniform) [24,49,50]
Fall time threshold	1000–5000 (uniform)
Lithic density	2500 kg/m^3 [52]
Pumice density	1400 kg/m^3 [52]
Column steps	150 Point source distance <167m
Particle steps	20 Bin width <0.65 ϕ
Plume model	Beta distribution α = 3, β = 1.5 The majority of mass is released at around 80% the total height

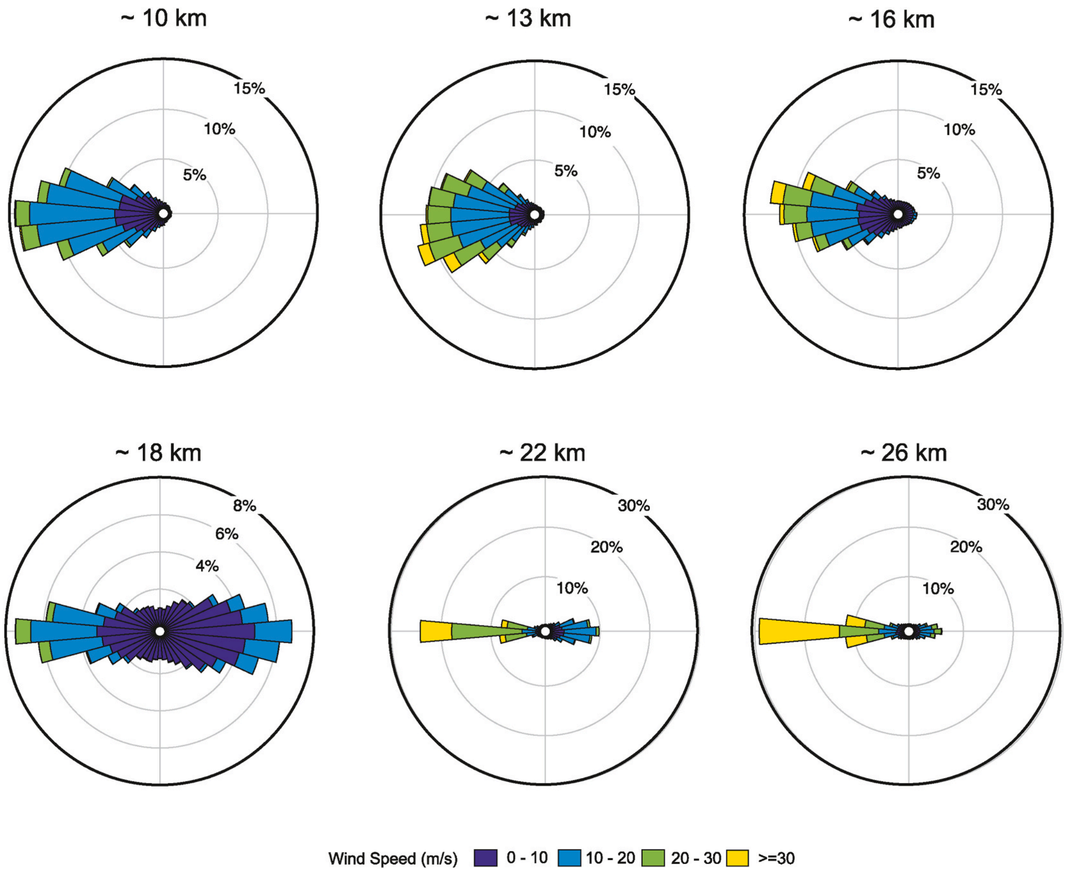

Fig. 3. Wind roses show the direction that the wind blows towards and the wind speed at various heights in the atmosphere (km above sea level). Wind data are sourced from ERA5 reanalysis dataset for the time interval 2014–2023 [51].

buildings are pre-dominantly single storey detached structures constructed with concrete block walls. Metal roofs are often gable or hip type with wooden supports. In many cases a ventilation gap was observed between the upper part of the front and rear walls and the roof, a feature intended to improve airflow. Field observations and visual inspection of Google Earth imagery shows that many of these metal roofs are heavily corroded. For metal sheet roofing the degree of corrosion influences vulnerability since corroded roofs have a higher coefficient of friction, meaning that tephra slides off less easily increasing the chance of failure, while also reducing the resisting strength of the material [15]. Based on this we focussed on identifying different roof types distinguishing between average-good (not corroded) and poor condition (corroded) metal roofs.

Field observations and satellite imagery also reveal the presence of brightly coloured blue or red roofs. These are made from sheets of zinc shaped to resemble traditional roof tiles and coated with an anti-corrosion layer. A common proprietary version of this material in Indonesia is marketed under the trademarked name Sakura Roof (PT Tatalogam Lestari; https://tatalogam.com/portfolio/sakuraroof). From hereon in we refer to this roof type as ‘Sakura’.

Sangihe Island has ~62,500 buildings (Google open buildings), given that building level characteristics are not available for the whole of the island, we developed exposure data by combining building footprints from the Google Open Buildings dataset [58] with PlanetLab optical satellite imagery (Red, Green, Blue colour bands, 4.5 m pixel spatial resolution; acquired November 2023).

In this work we therefore considered three roof types: (1) Sakura, (2) poor condition metal sheet, and (3) average-good condition metal sheet. For the calculation of financial losses, we applied the same building replacement value to all three types, as the roof category (whether its poor condition or average-good condition) affects vulnerability but not the underlying replacement cost of the building. Discussions held with staff at a building-material supply store in Tahuna during fieldwork also indicated that the cost of Sakura roofing is broadly comparable to that of standard metal sheet roofing, supporting the use of a uniform replacement value across roof categories.

To extract roof type information, we developed a method using pixel RGB colour values within each building footprint. Dark red roofs were classified as poor condition metal, bright grey as average-good condition metal, and non-grey bright colours as Sakura.

We manually labelled 1545 buildings in four 500 × 500 m areas across the island and extracted the median value for each of the RGB channels per building footprint using QGIS. We applied a two-stage classification: first, separating ‘brighter’ roofs (Sakura plus average-good condition metal) from ‘duller’ roofs (poor condition metal) using a brightness threshold based on the maximum of the median RGB values for each building footprint. This was identified via a 70/30 training-evaluation split. Using the same data split proportions, in the second stage, the threshold between Sakura and average-good condition metal roofs was identified by analysing the RGB band differences, since grey-coloured pixels exhibit lower inter-band variation. To ensure that the identified thresholds were not sensitive to the choice of data split we conducted K-fold cross validation for both stages with $K = 50$. For both of the two classifications we evaluated the performance of each fold by calculating the F1 score for each split; i.e., 1) bright coloured (Sakura and average-good condition metal) vs dull coloured (poor condition metal), and 2) low inter-band variation (average-good condition) vs high inter-band variation (Sakura). The F1 score ranges from 0 to 1 where 1 is a perfect classification and is calculated as follows:

$$F_1 = \frac{2 \times (precision \times recall)}{precision + recall}$$

2.3. Building vulnerability

The vulnerability of exposed assets can be described by fragility functions that are cumulative probability distributions that represent the probability of the asset exceeding a given damage state (severity) when subjected to a certain hazard intensity, for tephra fall this is usually loading (kPa or kg/m^2) (e.g., [15,29,59]). In absence of fragility functions specific to the regional building types found on Sangihe Island, to model the relationship between tephra loading and the expected damage for the three roof types identified, we sought to incorporate information from existing vulnerability models for building types as close as possible to those in the region. We identified two sets of suitable fragility functions for building types that are similar to those on Sangihe Island. The first set was developed under the framework of the MIAVITA project; Jenkins and Spence [60] used expert judgement to develop fragility functions for the probability of roof failure for five broad building classes (Atf, Btf, Dtf, Etf, Ftf). These broad classes grouped existing classifications from other authors developed for specific locations based on their vulnerability to tephra fall rather than specific construction styles or materials. The goal being that broad classes could be more widely applied. The Atf building typology includes: “Metal sheet roofs on timber rafters/trusses, in old or poor condition; Tiles on timber rafters/trusses, of old or poor condition”, this classification maps to the poor condition metal sheet roofs found on Sangihe Island. The Dtf typology in Jenkins and Spence [60] includes: “Metal sheet roofs in average condition; Tiles on timber rafters/trusses in average or good condition”, this classification maps to our average to good condition plus Sakura metal sheet roofs found on Sangihe Island. We grouped the Sakura with the average-good condition metal as the anti-corrosion coating meant that Sakura was usually in good condition. The second suitable vulnerability model set used was developed by Williams et al. [30] from a remote sensing damage assessment conducted after the 2014 eruption of Kelud, Indonesia. Functions describe the probability of different damage states DS2, DS3, DS4/5 (Table 1) for grey roofs (asbestos and metal sheet) and tiled roofs, which align with the Atf and Dtf global typologies [60]. Although both materials could be assumed to be in average condition and therefore suited to the Dtf class, evidence from Kelud shows that the grey roofs exhibit markedly higher vulnerability to tephra loading. Therefore, their observed behaviour aligns more closely with the Atf category of Jenkins and Spence [60].

Given that neither set of vulnerability functions was developed specifically for the regional building types found on Sangihe Island, but both sets can provide insight into how Sangihe Island's buildings may behave, we opted to combine information from both of the function sets. To generate these hybrid fragility functions we used Bayesian inference to update the two prior fragility functions from Jenkins and Spence [60] (Atf and Dtf) with new information in the form of the two DS4/5 curves from Williams et al. [30] (grey roof and tiled roof). The Jenkins and Spence curves were adopted as the prior model since they reflect expert-elicited, high-level estimates of tephra vulnerability and thus provide a reasonable first approximation for Sangihe's building stock. This prior was then updated with national data to obtain more refined vulnerability relationships. As no prior fragility functions exist for DS2 and DS3, we adopted the Williams et al. [30] models without updating. For each building and each hazard footprint the three fragility functions corresponding to that building type were applied to find the most likely damage state for the tephra accumulation received: the DS2 and DS3 functions from Williams et al. [30] and the updated DS4/5 functions.

2.3.1. Bayesian updating of tephra fall fragility functions

Bayesian inference provides a robust means of updating existing knowledge about a random variable with new knowledge. Applications in volcanology to date have included updating probabilities in event trees [61,62] and deriving frequency-magnitude relationships from analogue volcanoes [63].

To update the DS4/5 fragility functions we used a beta distribution to represent the prior (J&S [60]) and a binomial distribution for the ‘new’ data (Williams et al. [30]) respectively. The conjugate property of the two distributions means that the resultant updated posterior distribution is a beta distribution, a useful property when dealing with probabilities. For both poor and average-good condition metal typologies, we divided the J&S prior curves into bins of 0.1 kPa, an arbitrarily chosen bin value that was found to have no effect on the shape of the final posterior fragility curve. At each bin centre we extracted the fiftieth percentile probability (p_{50}), and the probabilities given by the confidence intervals in Jenkins and Spence [60] that are $\pm$ 1 standard deviation or the p_{18} and p_{84} percentile. For each bin we fit a beta distribution (beta [α_1 , β_1]) to the three percentiles by minimising the sum of the squared errors and, stored the fitted α_1 and β_1 parameters. For all bins, the beta distribution was a good fit and the calculated percentiles of sampled data from the fitted distribution matched the original percentiles from the confidence intervals.

For each bin centre we updated the α_1 and β_1 parameters using the new observations from the corresponding bin for the Williams curve. To convert the new data probabilities (p) extracted from the curve into binomial counts i.e., (X) successes and (N) trials we could obtain the same probability with denominators of various precisions, i.e., a probability of 0.45 could be obtained with $X = 45$, $N = 100$, or $X = 450$, $N = 1000$ and so on. The choice of N determines how strongly the new probability influences the update, higher values of N imply greater precision or confidence in the new data, with the updated posterior distributions more strongly reflecting the new data.

For each bin we set N as a function of the Williams' curves confidence bounds (i.e., $\text{Williams DS4/5}_{\text{upper}}$, and $\text{Williams DS4/5}_{\text{lower}}$) and a scaling factor S:

$$N = \frac{S}{\textit{Williams DS}4/5_{upper} - \textit{Williams DS}4/5_{lower}},$$

When S is 1 this represents the maximum confidence on the new data, and for $S < 1$ the confidence on the new data is reduced. To set S we determined that confidence would be higher for the non-extrapolated portion of the Williams' curve (up to ~1.45 kPa). We set S using the exponential decay function based on the distance in kPa (D) to the last bin with data

$$S = e^{-D}$$

We then used N to calculate X:

$$X = p \times N.$$

The updated posterior beta parameters for each bin were then calculated as follows:

$$\alpha_2 = \alpha_1 + X,$$

$$\beta_2 = \beta_1 + (N - X)$$

To ensure that our updated DS4/5 fragility functions are in line with the other functions in the set (DS2, DS3), for both of our updated functions we used the corresponding DS3 fragility functions to provide constraints on the update. If the updated DS4/5 curve intersected the DS3 curve the probability of DS4/5 is equal to the probability of DS3 and DS4/5 is taken as the more likely damage state.

3. Results

3.1. Tephra fall hazard

Hazard simulations show that tephra fall from a VEI 4 sized eruption at Awu is expected to affect much of Sangihe Island. The most likely dispersal axis is towards the west and the greatest accumulations are expected in this direction (Fig. 4). The town of Kendahe, located 6 km west of the summit in Kendahe district is almost certain (95% probability) to receive at least 100 kg/m^2 (Fig. 4c–f). The capital city of Tahuna, located ~8–11 km southeast from the volcano has a 30–50% probability of 10kg/ m^2 (Fig. 4b–e) and a 10–30% probability of 100 kg/m^2 (Fig. 4f). There is a low chance (5% probability) that an accumulation of at least 100 kg/m^2 could reach up to ~12 km away from the volcano covering the districts of Kendahe, Tahuna Barat, Tabukan Utara, Tahuna, and Tahuna Timur, and potentially affecting ~50% the total number of buildings on Sangihe Island (Fig. 4a). There is a 10% probability that an accumulation exceeding 1 kg/m^2 will extend to the southernmost point of the island, ~37 km from the volcano, and relatively upwind from the volcano (Fig. 4d).

3.2. Building exposure

Our method for extracting building typology information using satellite imagery and the Google building footprints performed well. F1 scores for poor condition metal, average-good condition metal, and Sakura were: 0.84, 0.71, and 0.79 respectively, overall accuracy on the full labelled dataset was 0.79 and the F1 score was 0.78. Mean and standard deviation of the F1 scores for K-fold cross validation for the first stage of classification which distinguished between dull coloured (poor condition metal sheet) vs bright coloured (combined average-good condition metal sheet and Sakura) were 0.81 (SD = 0.02), and 0.72 (SD = 0.03) respectively. Mean and standard deviation of the K-fold cross validation scores for the second classification which separated average-good condition metal sheet from Sakura were 0.97 (SD = 0.007) and 0.80 (SD = 0.04). The low standard deviation across the folds demonstrates that our approach was not sensitive to the training and testing split. Plots showing the F1 scores for each fold are given in the Supplementary material (Fig. S2).

Using the identified best thresholds, we classified all 62,512 building footprints located on Sangihe Island. We found that 67% of buildings have metal sheet roofs in poor condition, 29% have metal sheet roofs in average-good condition, and 4% have Sakura roofs. Fig. 5 shows that 55% of the total buildings on Sangihe are within 15 km of the volcano. Besides the 25–35 km distance bin, which covers the largest area due to the island's shape, the total number of buildings of any type decreases with distance from the volcano. At 5–10 km radial distance there are a greater number of buildings than any of the other distance bins. This area encompasses Tahuna district and the Northern part of the capital city by the same name which also extends into the 10–15 km bin. The proportion of good condition metal sheet roofs in the bins that encompass the capital (5–10 km and 10–15 km) is approximately double the proportion in the bins located farther away from the volcano, potentially due to greater economic input into the capital.

3.3. Bayesian updating of fragility functions

Fig. 6a and b shows the notable difference in the shapes of the Jenkins and Spence [60] prior curves and the Williams et al. [30] new

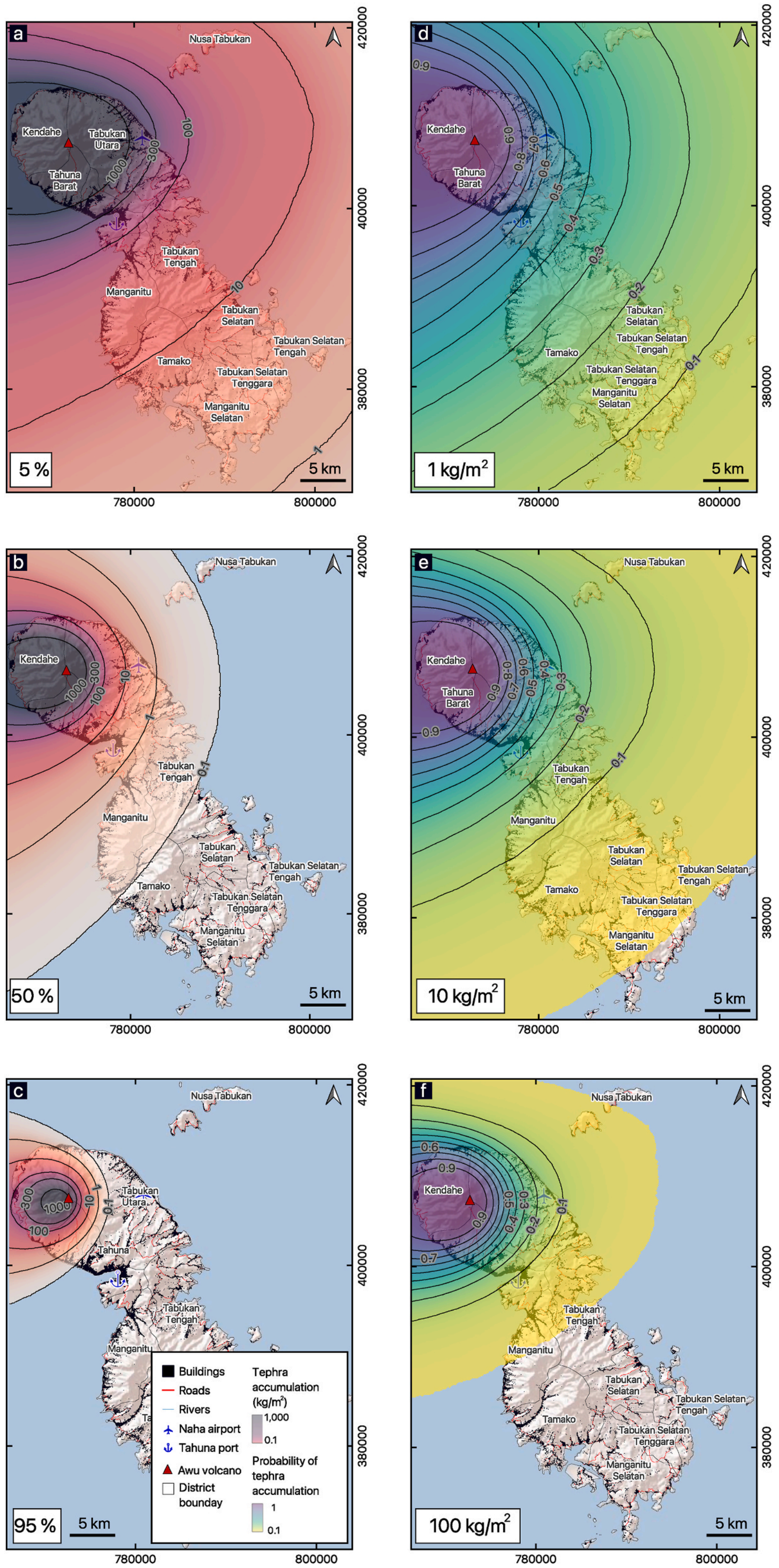

(caption on next page)

Fig. 4. a–c) Tephra accumulation from a simulated VEI 4 sized eruption of Awu volcano. Probabilistic isomass maps describe the tephra accumulation associated with a 5-50-95% exceedance probability, where the 5% isomass map is the tephra accumulation that is exceeded in 5% of simulations, equivalent to the 95th percentile of the hazard. d-f) Probability maps showing the conditional probability of accumulation that is at least 1, 10, 100 kg/m^2 following a VEI 4 sized eruption at Awu volcano. Simulations were conducted using Tephra2 within the TephraProb wrapper. Base map: ESRI shaded relief. Building footprints: Google Open Buildings. Coordinate reference system: EPSG: 32651.

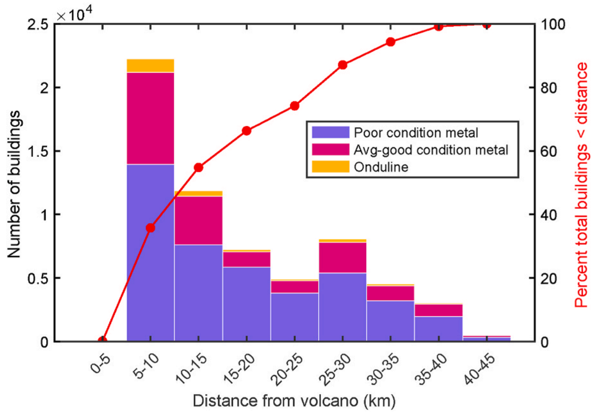

Fig. 5. The distribution of the three roof types with distance from Awu volcano and the cumulative percentage of buildings with distance from the volcano (right axis). 100% of buildings (N = 62,512) includes all buildings on Sangihe Island. All buildings have at least a 5% probability of an accumulation that is $\geq$ 1 kg/m^2.

data curves. Specifically, for both roof types, the [30] curve indicates higher exceedance probabilities at lower values of loading but lower probabilities at the higher end of the loading range compared to the Jenkins and Spence [60] curve. The models differ in their functional form and in the data used to develop them: the Jenkins and Spence [60] fragility curves use a cumulative lognormal distribution while the Williams et al. [30] curves were fitted using a cumulative link model. Expert judgement was used to combine existing models to generate the J&S curves, while the Williams curves were generated from field data collected after the Kelud eruption. The updated fragility functions that integrate prior data from the Jenkins & Spence (J&S) roof collapse curves with the DS4/5 curves from Williams et al. [30] achieve a balanced integration of these two curves. At lower loading levels, they align closely with the Williams et al. [30] curve, which was derived from observational data up to 1.45 kPa. As loading increases, and the influence of data diminishes, the updated curves gradually converge toward the prior J&S data, reflecting a transition to expert-derived estimates where empirical constraints are weaker (Fig. 6a and b). For the poor condition metal sheet roof, the DS4/5 curve meets but cannot cross the DS3 curve due to the constraints applied in our updating methodology (Fig. 6c). The full set of curves that were applied to the buildings on Sangihe Island comprising the updated DS4/5 curves and the DS2 and DS3 curves are shown in Fig. 6c and d.

3.4. *Forecasting tephra fall impacts*

Loss-exceedance curves describe the exceedance probability of different proportions of the total building stock having a damage state DS2, DS3, or DS4/5 given a VEI 4 sized eruption (Fig. 7a) and, the exceedance probability of losses in USD and IDR (Fig. 7b). From the 10,000 vulnerability samples for each hazard simulation, 10,000 loss-exceedance curves were produced. Fig. 7 displays the median and 5th–95th percentile confidence bounds; however, variability is minimal, and the confidence bounds overlap the median curve. The loss-exceedance curve for $\geq$ DS2 is very close to the $\geq$DS3 curve, because no buildings had a most likely damage state of exactly DS2 across the 100 million damage states calculated for each building. We attribute this to the high vulnerability of buildings on Sangihe Island.

We found that given a VEI 4 sized eruption scenario at Awu, it is likely (75% exceedance probability) that at least 5% of buildings will suffer heavy damage (DS $\geq$ 3) and 3% will experience severe damage or collapse (DS4/5). There is a remote chance (5% exceedance probability) that up to 40% of buildings may reach DS $\geq$ 3, with 20% suffering DS4/5 damage (Fig. 7a). Financial losses from damage or destruction of the building stock are expected to be significant. There is a 95 % probability that losses of at least ~$11 million USD (~179 billion Indonesian Rupiah [IDR]) will occur. This is equivalent to approximately 3% of the Sangihe Islands regency Gross Regional Domestic Product (GRDP = ~$364 million USD, [64]). There is a 75 % probability that losses will exceed ~$25 million USD (~407 billion IDR) (Fig. 7b). Under a low likelihood but high impact scenario (5% exceedance probability) losses of ~ $165 million USD (~2.7 trillion IDR) are expected to occur (Fig. 7b), equivalent to ~45% of the regencies GRDP.

The 50th percentile of the total financial losses calculated from the set of 100,000,000 unique calculations (10,000 hazard by 10,000 vulnerability) is ~$39 million USD (~649 billion IDR). In contrast, the financial losses calculated using the 50th percentile tephra accumulation footprint are 5% higher at ~$41 million USD (~682 billion IDR).

To understand the spatial distribution of losses across the island, and to identify areas that might be important for prioritisation of

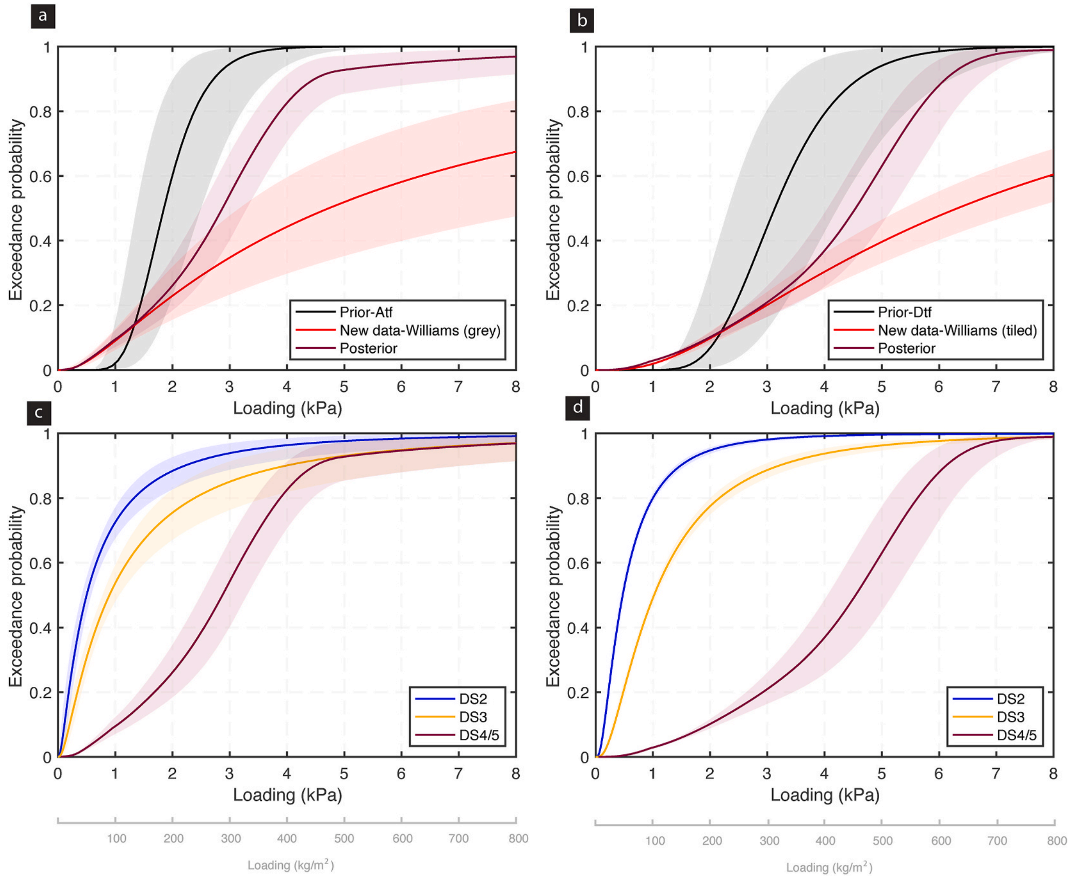

Fig. 6. a,b) The prior, new data, and updated posterior fragility functions for poor condition, and average-good condition metal sheet roofs respectively. Prior functions are from Jenkins and Spence [60], and the new data functions are from Williams et al. [30]. Confidence intervals are ± 1SD. c, d) The full set of functions applied to buildings on Sangihe Island. The DS2 and DS3 functions for both roof types are from Williams et al. [30], and the updated DS4/5 curves are derived through updating the [60] prior functions that describe the probability of roof collapse with the DS 4/5 functions from Williams et al. [30].

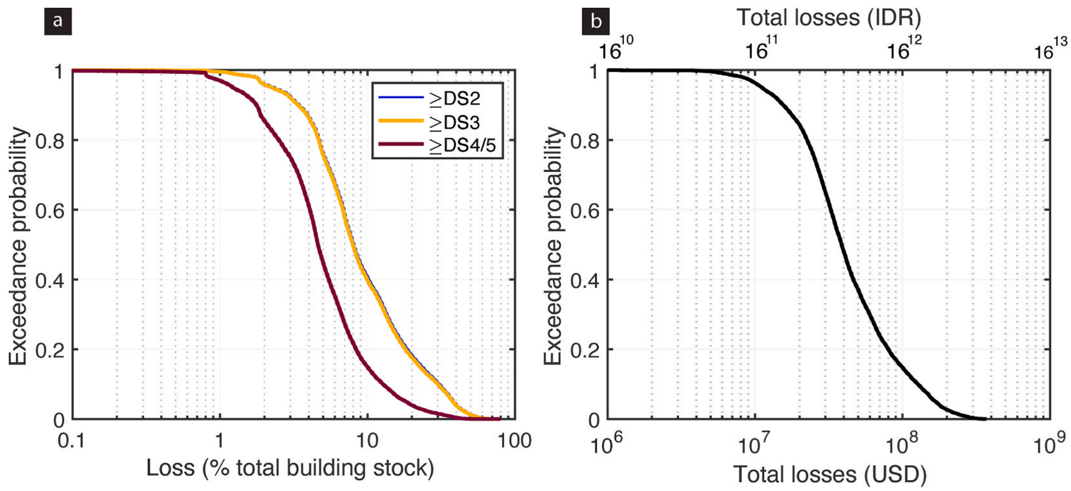

Fig. 7. Loss-exceedance curves show a) The exceedance probability of the % of the total building stock that has a damage state (DS) that is greater than or equal to DS2, DS3, DS4/5 given a VEI 4 eruption, note that the curve for ≥ DS2 is overlaid by the curve for ≥ DS3; b) The probability that the total losses in US dollars and Indonesian Rupiah are greater than the values on the X axis given a VEI 4 eruption.

mitigation strategies and/or recovery needs we calculated the losses for each of Sangihe Islands 12 districts plus the Nusa Tabukan island group (~5 km to the north) separately and computed the losses per district at a range of percentiles to show the uncertainty (Fig. 8). Forecasted losses are greater in the northern half of the island which is closer to the volcano and has a greater concentration of buildings. The 5th percentile calculated for each district suggests that it's very likely that losses of at least ~\$5 million USD (~81 billion

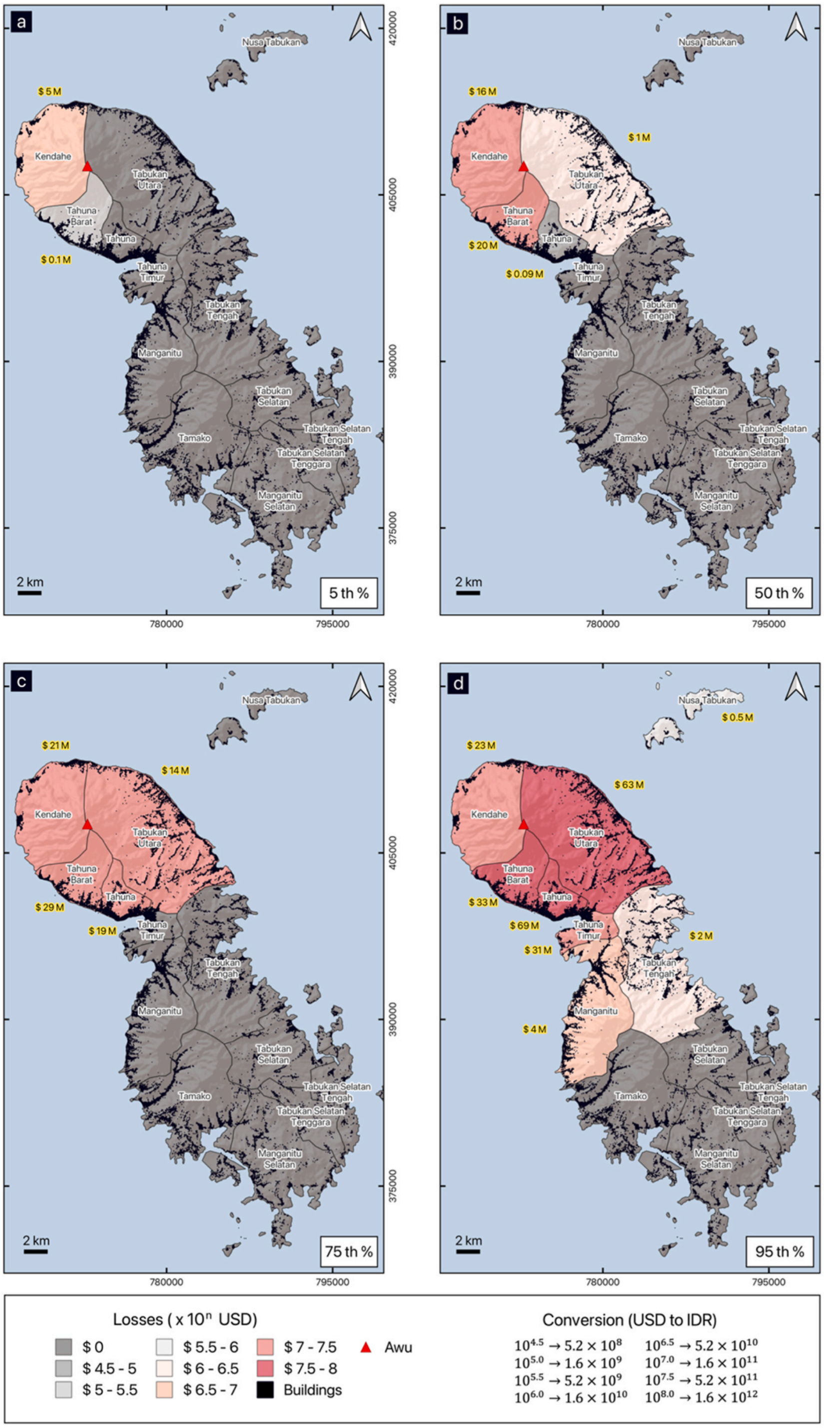

Fig. 8. Forecasted tephra fall-related losses to buildings on Sangihe Island from a VEI 4 eruption, shown per district for the 5th (a), 50th (b), 75th (c), and 95th (d) percentiles of total estimated losses. Colours show the value of the exponent, i.e., red coloured districts have losses of $10^{7.5}$- 10^{8} USD. Losses are based on 100 million simulations (10,000 hazard scenarios × 10,000 vulnerability realisations). Base map: ESRI shaded relief. Building footprints: Google Open Buildings. Coordinate reference system: EPSG: 32651.

IDR) will be experienced in Kendahe, and ~$0.1 million USD (~1.63 billion IDR) in Tahuna Barat (Fig. 8). The 50th percentile scenario shows that Tahuna Barat, Kendahe, Tabukan Utara and Tahuna are all likely to incur losses, with Tahuna Barat being the worst affected (>$20 million USD/326 billion IDR). While it is unlikely (95th percentile), it is possible that eight of the thirteen districts will experience significant financial losses from tephra fall. The 95th percentile losses are greatest in Tahuna, with ~$69 million USD (~1.1 trillion IDR), followed by Tabukan Utara with ~$63 million USD (~1 trillion IDR) (Fig. 8).

3.5. Understanding the drivers of loss

Estimating potential losses from known eruption characteristics can help guide emergency management planning and support the development of risk transfer solutions such as parametric insurance models. During an eruption the time of year (month)–which can be considered a proxy for the wind direction–is a known variable, while information about the column height is often quickly available through visual and satellite observations. Examination of losses as a function of column height shows that, broadly speaking, a greater column height is likely to result in more significant average losses as shown by the increase in the median losses per height bin (Fig. 9a). The median of the losses for a 11–12 km column is ~ $28 million USD (~453 billion IDR), for a 17–18 km column it is ~ $35 million (~567 billion IDR), and for the maximum plume height bin 25–26 km the median losses are ~$56 million (~907 billion IDR). A greater column height also results in increased variability in the losses, as shown by the increased distance between the median and 95th percentile with column height (Fig. 9a). The 95th percentile losses for these plume heights are ~$89 million, ~$157 million, ~ $233 million respectively. The relationship between column height and losses is not linear since similar total losses can be achieved with different column heights (Fig. 9a). This complexity is highlighted by several examples; the bimodality in the upper column height bins (25–26 km and 26–27 km), which is related to differences in the erupted mass; and the lower median losses for the 19–20 km

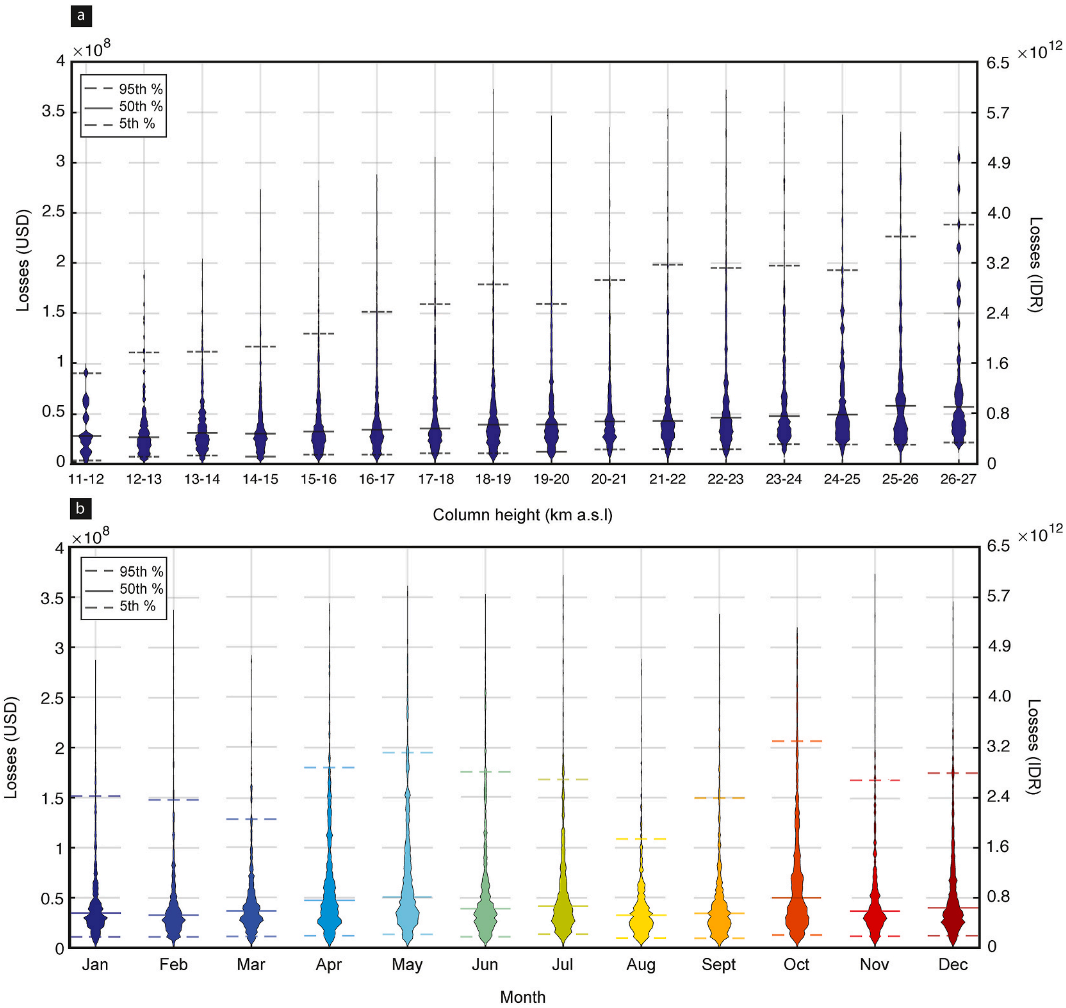

Fig. 9. Forecasted tephra fall-related losses to buildings on Sangihe Island from a VEI 4 eruption. Losses are in US dollars and Indonesian Rupiah displayed as a function of a) column height (km above sea level) and b) month. Dashed and solid lines represent the 5th, 50th, and 95th percentiles of the data.

column height than the 18–19 km height.

Examination of the losses as a function of the month suggests that median losses vary between ~\$32 million USD (~518 billion IDR) in February and ~\$50 million USD (~810 billion IDR) in May, followed by ~\$49 million USD (~810 billion IDR) in October and ~\$47 million USD (~761 billion IDR) in April. Extreme losses (95th percentile) are greatest in October followed by May and April (Fig. 9b), however similarly to the relationship between column height and losses, this is not linear.

While some general observations can be made about the relationship between losses and column height or month (Fig. 9), to further understand the conditions that control the losses we extended this analysis to consider other ESPs. The Pearsons correlation coefficient (Pearsons R) describes the linear relationship between variables, where 1 is a perfect positive correlation and −1 is a perfect negative correlation. The Pearsons R values for the correlation between the main ESPs and the losses suggests that no single parameter is well correlated with the losses, though erupted mass has the highest R value (Table 3). Generally, a higher erupted mass (left to right across the five mass intervals, Fig. 10) results in greater losses, as does a finer median grain size (top row to bottom row) and a greater column height (bottom to top for each row). However, Fig. 10 also highlights the interactions between parameters; for example, the maximum mass bin combined with the minimum grain size and the maximum column height row, which theoretically should result in the maximum average losses, instead results in average losses at the lower end of the losses range in March and May, and the upper end in April. Comparatively high average losses can occur for low plume heights with a low erupted mass, but a fine median grain size (Fig. 10).

3.6. *Investigating extreme impact scenarios*

Extreme impact scenarios have losses that are greater than the 95th percentile of the full loss dataset (\$165 million USD/2.67 trillion IDR). For the 500 hazard simulations in this extreme impact subset we found that the median column height and erupted mass were greater and the median grain size finer than in the full dataset (Fig. 11). For the column height, 75% of the extreme impact subset had a height greater than 18 km asl and a median grainsize smaller than −1 phi. The lowest column height within the extreme impact subset was 12 km asl, close to the minimum simulated 10 km, however the very fine median grain size (0.9 phi) and the occurrence of this simulation in April likely contributed to the high losses. The extreme impact subset is not dominated by any single month, though October (16%), May (13%), and April (11%) account for the highest proportions (Fig. 11). These same months also correspond to the greatest average losses (Fig. 9b). While the erupted mass seems to have the greatest control on the losses for both the full set of simulations and for the extreme impact subset (Table 3), for the full set the second most important parameter is the column height, while for the extreme impact subset the second most important ESP is the median grain size (Table 3). This observation is also highlighted by the greater separation between the medians of the full loss dataset and extreme impact subset for the median grain size than the separation for the column height.

The ESPs associated with the top ten hazard simulations that produced the greatest financial losses demonstrate the specific combinations of eruption source parameters and wind conditions that lead to the greatest losses (Fig. 12). Combined ESPs and wind conditions that lead to extensive tephra deposition towards the southern part of the island rather than the more likely western direction are responsible for these maximum credible impact cases. Fig. 12 shows the extent of the 285 kg/m^2 contour, which is sufficient to have a 50% exceedance probability of DS4/5 for the more common poor condition metal sheet roof. In the most extreme cases, sufficient accumulation for a 50% exceedance probability of DS4/5 can reach ~21 km from the volcano.

4. Discussion

4.1. *Interpretation of the main findings*

Our analysis indicates that a VEI 4 eruption of Awu volcano would result in widespread tephra fall impacts to buildings. Despite dominant westward wind conditions transporting much of the tephra offshore, the small size of Sangihe Island means that nearly all of the island's 62,512 buildings, which lie within 45 km of the vent, will experience some tephra fall. The majority (67%) of buildings have relatively weak roofing material (corroded metal). As a result, when the modal damage state is assigned to each building based on the 100 million simulated damage states, all damaged buildings (N = 3895) are forecast to have heavy to severe damage (DS3 or DS4/5).

In Kendahe district, which lies directly west of Awu, it is almost certain that a high proportion of buildings will be damaged from tephra fall, but the comparatively lower number of buildings (N = 2399) means that the dollar losses are not as high as in other

Table 3
Pearsons correlation coefficients (R value) describe the linear correlation between Tephra2 eruption source parameters (ESPs) and the calculated financial losses due to building damage from a VEI 4 sized eruption. Shown are the coefficients for the full loss dataset consisting of 10,000 unique ESP combinations, and the ESPs for the extreme impact subset that consists of hazard simulations where losses are greater than the 95th percentile (N = 500). For all, the correlations were statistically significant (p value < 0.05).

Eruption source parameter	Pearsons R value (full loss dataset)	Pearsons R value (extreme impact subset)
Erupted mass	0.32	0.33
Column height	0.23	0.20
Median grain size	0.12	0.26

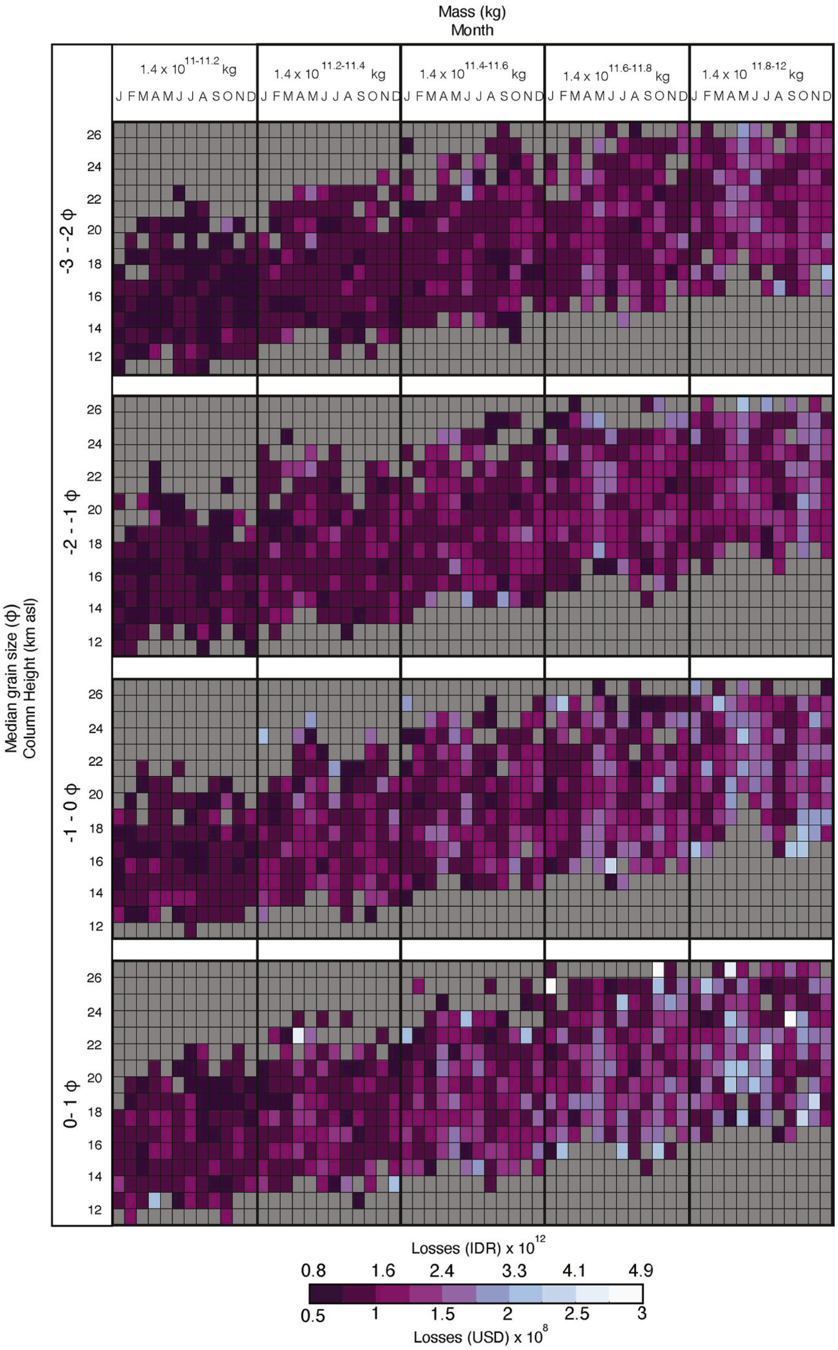

Fig. 10. Coloured cells show the losses for the different combinations of eruption source parameters: the mass, month, median grain size, and column height. Each cell represents the mean of the losses for the parameter combination. Grey cells represent no data, i.e., no simulations for the specific parameter combinations.

districts. Districts expected to incur the greatest financial losses are those with both proximity to the volcano and high building numbers. Notably, despite having a greater overall proportion of average-good condition metal sheet roofs (Table S1) the district of Tahuna, ~8–11 km from the volcano and home to the island's capital, has one of the highest building number counts (N = 8687), making it especially susceptible to substantial economic loss.

Forecasted losses assume that no mitigation measures have been put into place to reduce the damage. Measures taken during past eruptions elsewhere that could be employed at Awu include cleaning tephra off roofs, internal propping of roof beams, or covering the roof in tarpaulin to help tephra slide off (e.g., [56,65]). Our exposure analysis found that the majority of metal roofs were heavily

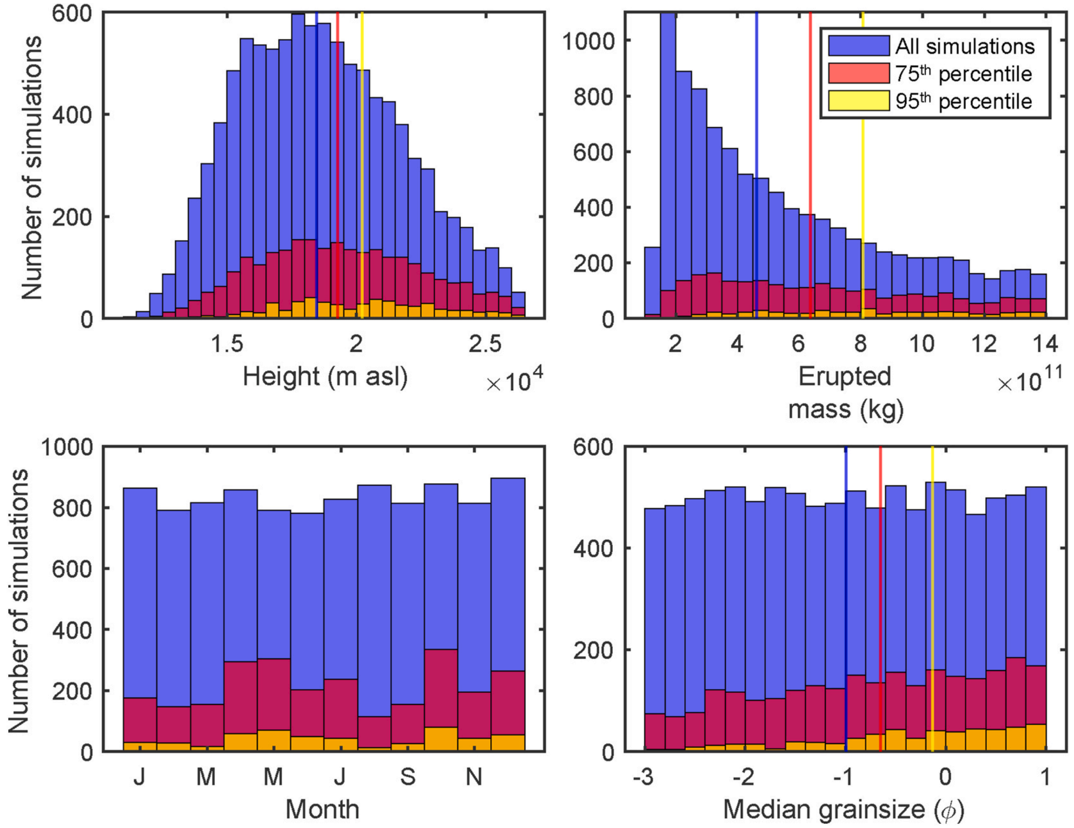

Fig. 11. Histograms show the Tephra 2 eruption source parameters for all 10k hazard simulations, and the parameters that contributed to the 75th percentile and 95th percentile (extreme impact subset) of the losses. Vertical lines mark the median of the corresponding data subsets.

corroded, investment in replacing existing corroded roof coverings with material that is less susceptible to corrosion such as the Sakura material may also help to reduce future losses.

The current operational long-term hazard map for Awu is based on eruptive history and field studies which were used to define three hazard zones [66]. Volcanic Hazard Zone I marks an 8 km radius around the crater as the area potentially affected by heavy ashfall and ejected material based on expert synthesis of past tephra fallout extents. Despite fundamental differences in purpose and underlying datasets, our simulations are broadly consistent with this, indicating that the 8 km boundary roughly corresponds to a 50% probability of exceeding 10 kg/m^2 and a 20% probability of exceeding 100 kg/m^2.

During the most recent VEI 4 eruption of Awu in 1966, tephra fall damage was reported in Kendhar (Kendahe) and Talawid villages [37]. These villages are directly west of the volcano, consistent with the prevailing wind direction in our simulations. We found that there is a 90% probability of 285 kg/m^2 (the median load associated with heavy damage to poor condition metal sheet roofs) at Kendahe and a 70% probability of this loading at Talawid. In total, 3045 buildings were reported destroyed during the 1966 eruption [37]. Under present-day exposure conditions, our modelling suggests an approximately 75% probability of a comparable number of buildings experiencing damage states of DS $\geq$ 3 from tephra fall alone. However, historical accounts also report damage from pyroclastic density currents in Kendahe, and in coastal villages in the north and east during this eruption [37], indicating that multiple hazards likely contributed to the observed building losses. A more recent comparison can be drawn with the 2021 VEI 4 eruption of La Soufrière volcano, St Vincent and the Grenadines, that resulted in direct losses to the housing sector of ~$12 million USD [67]. Based on our analysis there is a 94% probability that losses from a VEI 4 sized eruption at Awu will exceed this amount. Both islands have similar building numbers and relatively small land area: St Vincent Island (~42,000 buildings, [Open Street Map, 2023] over ~390 km^2) and Sangihe Island (~62,500 buildings over ~740 km^2). Despite the higher average replacement cost in St Vincent and the Grenadines [68], losses are expected to be greater at Awu, likely due to variation in building exposure and vulnerability. Sangihe Island's capital which spans the districts of Tahuna, Tahuna Timur and Tahuna Barat, and hosts ~30% of Sangihes total buildings, is closer to the volcano (~8–11 km vs ~20 km for St Vincent), while visual inspection suggests that the majority of roofs on St Vincent are made of good condition metal with limited corrosion [69] making them less vulnerable to damage.

Our work has shown that while there are some broad trends, losses at Awu are not well forecasted by column height and eruption timing (month) alone. Instead, they reflect interactions between erupted mass, column height, median grain size, and eruption timing. In contrast, a study of eruptions affecting Tokyo and Kanagawa prefectures in Japan has shown a correlation between column height, wind conditions, and financial losses [28]. This relationship has been proposed as the basis for triggering volcanic parametric

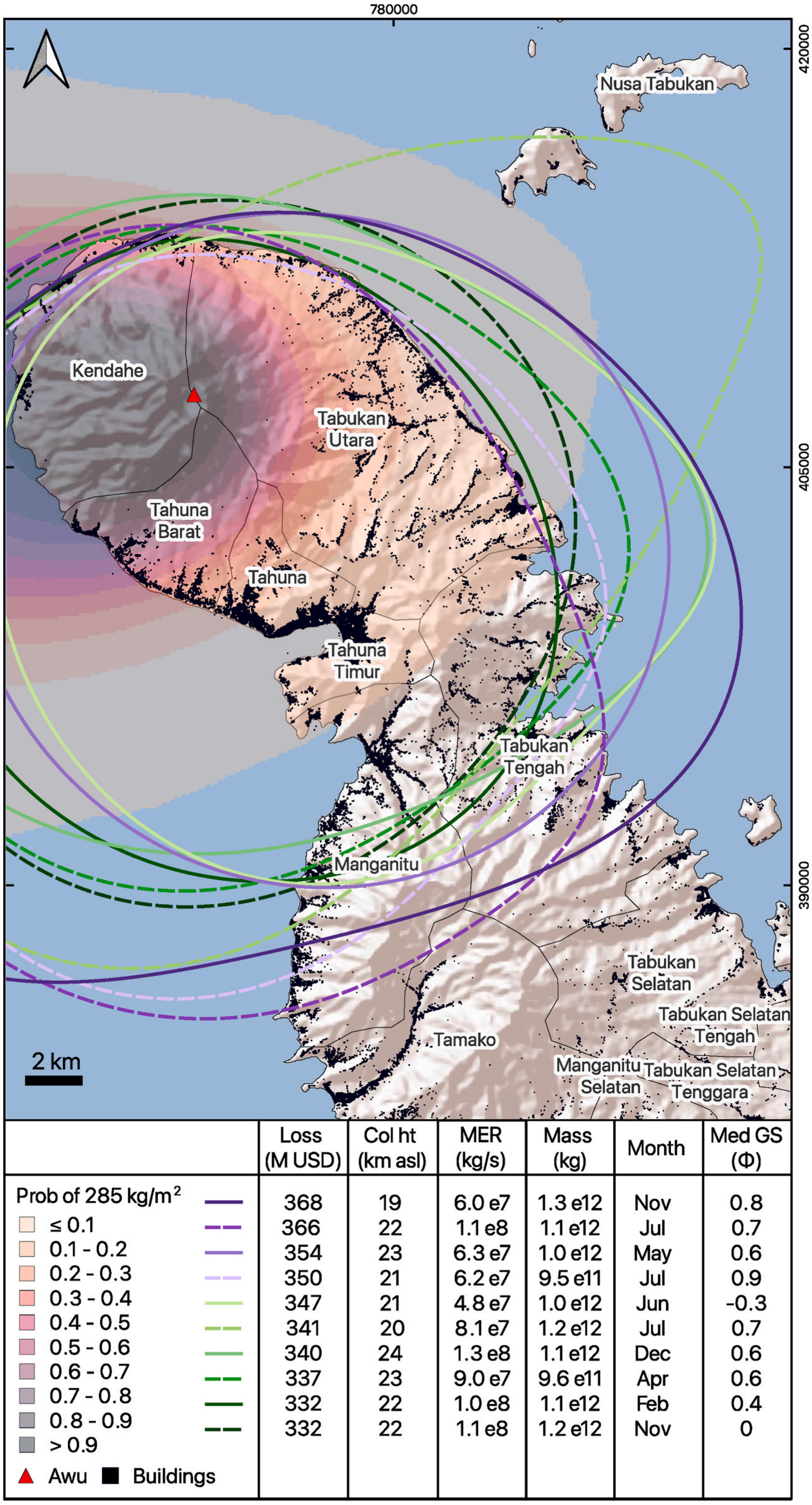

Fig. 12. Individual hazard footprints for tephra accumulation exceeding 285 kg/m^2 (the median load associated with heavy damage to poor condition metal sheet roofs) for the ten greatest (max \$) loss scenarios. Base map: ESRI shaded relief. Building footprints: Google Open Buildings. Coordinate reference system: EPSG: 32651.

catastrophe risk bonds, insurance instruments that enable rapid post-disaster payouts when certain hazard thresholds are exceeded. Our findings suggest that this relationship may not be true for Awu. The relative proximity of buildings on Sangihe Island to the volcano potentially reduces the influence of individual parameters, resulting in losses that affect most areas and are less dependent on specific eruption parameters. These insights suggest that a parametric trigger based on column height and time of year may not be suitable for losses from a VEI 4 sized eruption of Awu. It is not clear what might be a suitable trigger for Awu, with multiple factors appearing to influence loss. More generally, further research is needed to evaluate how well parametric triggers relate to loss at active volcanoes worldwide.

While this work focusses on tephra fall impacts to buildings, our hazard simulations indicate the potential for broader impacts to other exposed assets. There is at least a 10% probability of tephra accumulation exceeding 1 kg/m^2 across most of Sangihe Island, and at least a 10% probability of accumulation exceeding 10 kg/m^2 across the northern half. Although generally below thresholds for structural damage, these accumulations can reduce road traction, obscure surface markings, disrupt power and telecommunication networks, and hinder agricultural productivity, particularly during harvest operations [70–73]. Future work might consider the quantification of impacts to these assets and the quantification of potential impacts from other hazards, particularly PDCs and lahars since these have historically caused the most fatalities at Awu ([34,38]). Multi-hazard, multi-asset risk assessment can be facilitated by dedicated frameworks (e.g., CAPRA, [74]; ADVISE, [75]; RiskScape, [76]; OpenQuake, [77]) however these are currently set up to handle a single hazard footprint.

4.2. Methodological considerations

4.2.1. Quantification of uncertainty

Pre-event impact forecasting has uncertainty associated with each of the constituent components of hazard, exposure, and vulnerability [24]. In this work we aimed to account for some of this by running probabilistic simulations across the hazard and vulnerability components. We found that uncertainty in the vulnerability functions had a minimal impact on loss estimates for Awu, likely due to the tight confidence intervals on the curves at the tephra loading range received, although this observation is likely to be case specific. There is a 5% discrepancy between the 50th percentile of the modelled losses (~$39 million USD) and the losses calculated at the 50th percentile hazard footprint (~$41 million USD). This highlights the uncertainty associated with application of semi-probabilistic approaches that calculate losses using a single Nth percentile hazard footprint (e.g., [10,13,24,26]). For tephra fall impacts to buildings at Awu the losses were overestimated using the 50th percentile hazard footprint; this contrasts with the findings of Williams [78] who showed that losses calculated for Kelud volcano, Indonesia were underestimated using the 50th percentile footprint. More work is needed to understand the specific hazard and exposure characteristics that affect whether losses can be approximated using the Nth percentile hazard footprint.

4.2.2. Building exposure

In the absence of detailed building-level exposure data for Sangihe Island, we used a straightforward approach, thresholding satellite optical imagery to classify roof types within building footprints into three typologies. While more advanced machine learning techniques are increasingly becoming available for building exposure mapping (e.g., [79–81], with performances of: accuracy = 0.81; F1 = 0.96; and accuracy = >0.8 respectively); our method achieved comparable performance, with an overall accuracy of 0.79 and F1 score of 0.78. While we consider this to be good, we expect that the use of higher resolution imagery (>4.5 m) would lead to improved classification. In this work we focussed on differentiating different roof covering types and conditions on the basis that the degree of corrosion of metal sheet roofs affects vulnerability to tephra fall damage [15]. With higher resolution imagery future work could employ machine learning to extract additional building features relevant to tephra fall vulnerability such as roof type (gable, hip, flat etc), pitch, and material [5,15,54,82]. However, these methods also require large, diverse, and labelled image datasets, which are often resource-intensive to compile. More data are needed not only to train models for extracting building characteristics but also to develop vulnerability relationships that account for these characteristics. While intra-class variability is accounted for to some extent by the uncertainty bounds in vulnerability models these are not always provided in published models, something that has been highlighted as a key priority for future model development [17].

To calculate losses, we used a building replacement value of $12,000 USD and assigned each damage state a proportion of this value (after [46]), while our damage state counts are not affected by these choices our final calculations of financial losses are undoubtedly sensitive to this. Future analysis might consider assigning replacement costs as a function of the total floor area of buildings that might be derived from the building footprints, and the height of buildings that could be assigned through disaggregation of remotely sensed datasets (e.g., [83]).

The replacement value was identified by local experts during a workshop held in April 2025. In a preliminary analysis we used information from the Global Exposure Model (GEM) dataset. We calculated the weighted average replacement cost for residential buildings on Sangihe Island from the GEM dataset as $38,000 USD. In the GEM dataset, 76% of residential buildings on Sangihe fall into one of three typologies based on construction style: confined masonry ($48,000 USD), unreinforced masonry ($17,000 USD), and wood (~$13,000 USD). The higher replacement values in the GEM dataset may partly reflect the inclusion of contents within the GEM provided replacement cost and the assumption of a "build back better" strategy where buildings are reconstructed to improved standards rather than restoring them to pre-event conditions. However, this strategy is not always consistently implemented in practice [68]. While GEM data provides valuable regional generalisations, it may not always capture local construction practices, material availability, or economic constraints specific to Sangihe. This highlights the critical importance of incorporating local knowledge into risk assessments to ensure that loss estimates, and recovery planning are both accurate and contextually appropriate.

4.2.3. Building vulnerability

Given the lack of vulnerability functions tailored to Sangihe Island's building stock, we adopted a Bayesian updating approach to combine information from existing functions developed for building typologies with similar vulnerabilities. Our approach uses building roof covering types to align the buildings on Sangihe Island with other available functions in terms of their vulnerability. In addition to the roof covering type the building construction style and materials influence the vulnerability to tephra loading.

In the Bayesian updating method we combined a cumulative lognormal prior model [60] with a cumulative link model [30]. Several challenges emerged in this process. First, the differing functional forms of the two models (lognormal vs. cumulative link) prevented conventional Bayesian updating of the prior model parameters. Second, attempts that refit both models within a common beta prime framework were unsuccessful, as the alpha and beta parameters differed by orders of magnitude, resulting in an unintended bias towards the model with tighter parameter distributions. Third, although updating the prior with raw data from Williams et al. [30] was considered - an approach taken by Bruijn et al. [84] and Tekeste et al. [85] - the narrow loading range of the data caused the posterior function to closely resemble the prior, without sufficiently addressing suspected limitations of the model. In particular, the prior was thought to underestimate damage probabilities at lower loading levels and overestimate them at higher loadings. To overcome these limitations, we adopted a hybrid strategy, extracting discrete data points from both models across the full loading range and updating fragility estimates at specific intervals (after [86]). While acknowledging the inherent challenges of combining models with fundamentally different structures and data characteristics, this approach allowed for a more balanced integration of the two datasets. In settings where fragility curves follow the same functional form and have broader overlapping ranges, parameter-based updating of the entire curve may be feasible. This is the first time that Bayesian updating has been applied to volcanic fragility functions and is a useful way of combining disparate data sources when typology specific functions are not available.

5. Conclusions

This study presents the first probabilistic assessment of potential impacts from a VEI 4 sized eruption at Awu volcano, which is currently experiencing heightened unrest. Despite prevailing westward winds, the small size of Sangihe Island means that nearly all buildings would likely be affected, with widespread structural damage due to the dominance of vulnerable roofing materials. Our findings indicate that financial losses are expected be substantial, particularly in Tahuna, and could exceed those observed during the VEI 4 2021 La Soufrière eruption in St. Vincent, despite higher building replacement costs there. This highlights the critical role of coupling hazard with local exposure and vulnerability information in shaping volcanic risk.

In contrast to other studies that have linked column height and wind conditions to the expected losses, we found that losses at Awu are not well forecasted by these parameters alone, instead specific interactions between column height, eruption mass, grain size, and the eruption timing – used as a proxy for wind conditions – control the losses. This finding suggests that triggers for parametric insurance payouts from volcanic eruptions, which are typically based on column height, wind conditions, may not hold in some contexts, and should be adapted for specific locations.

A key innovation of this work was the full integration of hazard, exposure, and vulnerability information to generate 10,000 × 10,000 loss estimates, that captured uncertainty in the analysis. This approach contrasts with more common 'semi-probabilistic' methods that estimate losses from a specific percentile hazard footprint. Our findings demonstrate that reliance on such approaches can result in differences in calculated losses, underscoring the need for fully integrated probabilistic analysis.

To overcome data limitations, we developed new methods to derive building exposure information from satellite imagery and refined vulnerability estimates using Bayesian updating of fragility functions. These methodological advances not only enable valuable insights into the potential impacts of a future eruption at Awu volcano but provide a template for risk assessments in other data-scarce settings. By delivering the first comprehensive, uncertainty-integrated volcanic risk assessment for Awu, this work provides a foundation for strengthening preparedness, guiding response planning, and building long-term resilience across Sangihe Island.

CRediT authorship contribution statement

Eleanor Tennant: Writing – review & editing, Writing – original draft, Methodology, Investigation, Formal analysis, Conceptualization. **Susanna F. Jenkins:** Writing – review & editing, Supervision, Methodology, Funding acquisition, Conceptualization. **Christina Widiwijayanti:** Writing – review & editing. **Ahmad Basuki:** Writing – review & editing, Conceptualization. **Heruningtyas D. Purnamasari:** Writing – review & editing, Conceptualization.

Funding

This research was supported by the Ministry of Education, Singapore, under its MOE Academic Research Fund Tier 3 InVEST project (Award MOE-MOET32021-0002) and the AXA Joint Research Initiative. This work comprises EOS contribution number 664.

Declaration of competing interest

The authors declare that they have no known competing financial interests or personal relationships that could have appeared to influence the work reported in this paper.

Acknowledgements

We are grateful for the valuable discussions on Awu volcano that took place during the hazard workshop held in Bandung, April 2025, with special thanks to Nugraha Kartadinata, Kristianto, Kushendratno, Hetty Triastuti, Soelistiyani, Yasa, David Adriansyah, Agoes Loekman, Edi Prantoko, Sofyan Primulyana, Ailsa Naismith, and Mieke Buckley. We extend our additional thanks to Kushendratno, Edi Prantoko, and David Adriansyah for generously sharing their expertise during fieldwork on Sangihe Island. We are also indebted to Mark Bebbington, Maricar Rabonza, and Giuseppe Petrillo for insightful discussions on fragility functions. Finally many thanks to the editor, Vitor Silva, and to two anonymous reviewers for their valuable feedback.

Appendix A. Supplementary data

Supplementary data to this article can be found online at https://doi.org/10.1016/j.ijdrr.2026.106040.

Data availability

Data will be made available on request.

References

[1] United Nations Office for Disaster Risk Reduction (UNISDR), Making development sustainable: the future of disaster risk management. Global Assessment Report on Disaster Risk Reduction, 2015.
[2] World Meteorological Organization, WMO Guidelines on multi-hazard Impact-based Forecast and Warning Services (WMO-No. 1150), 2015. Geneva.
[3] F. Lavigne, Lahar hazard micro-zonation and risk assessment in Yogyakarta city, Indonesia, Geojournal 49 (2) (1999) 173–183, https://doi.org/10.1023/A:1007035612681.
[4] W.P. Aspinall, G. Wadge, Risk assessment case history: the soufrière hills volcano, Montserrat, in: Global Volcanic Hazards and Risk, Cambridge University Press, 2015, pp. 343–348, https://doi.org/10.1017/CBO9781316276273.023.
[5] A.A. Pomonis, R. Spence, P. Baxter, Risk assessment of residential buildings for an eruption of Furnas Volcano, Sao Miguel, the Azores, J. Volcanol. Geoth. Res. 92 (1999) 107131, https://doi.org/10.1016/S0377-0273(99)00071-2.
[6] H. Rahadianto, H. Tatano, M. Iguchi, Multiscale impact assessment of massive ash fallout from a large eruption: what may happen if Sakurajima Taisho eruption occurs in contemporary Japan? J. Disaster Sci. Manag. 1 (2025) 24, https://doi.org/10.1007/s44367-025-00023-1.
[7] R.J.S. Spence, P.J. Baxter, G. Zuccaro, Building vulnerability and human casualty estimation for a pyroclastic flow: a model and its application to vesuvius, J. Volcanol. Geotherm. Res. 133 (2004) 321–343, https://doi.org/10.1016/S0377-0273(03)00405-0.
[8] M.A. Thompson, J.M. Lindsay, T.M. Wilson, S. Biass, L. Sandri, Quantifying risk to agriculture from volcanic ashfall: a case study from the Bay of Plenty, New Zealand, Nat. Hazards 86 (2017) 31–56, https://doi.org/10.1007/s11069-016-2672-7.
[9] I. Alberico, P. Petrosino, L. Lirer, Volcanic hazard and risk assessment in a multi-source volcanic area: the example of Napoli city (Southern Italy), Nat. Hazards Earth Syst. Sci. 11 (2011) 1057–1070, https://doi.org/10.5194/nhess-11-1057-2011.
[10] S. Biass, C. Frischknecht, C. Bonadonna, A fast GIS-based risk assessment for tephra fallout: the example of Cotopaxi volcano, Ecuador-Part II: vulnerability and risk assessment, Nat. Hazards 64 (2012) 615–639, https://doi.org/10.1007/s11069-012-0270-x.
[11] C. Muryani, Sarwono, R. Noviani, R.N. Azizah, Disaster risk analysis of Merapi Volcano eruption in the north slope based on the New Volcanic Risk Ranking (VRR) methods, in: IOP Conference Series: Earth and Environmental Science, Institute of Physics, 2024, https://doi.org/10.1088/1755-1315/1314/1/012015.
[12] M.-P. Reyes-Hardy, L.S.D. Maio, L. Dominguez, C. Frischknecht, S. Biass, L.F. Guimarães, A. Nieto-Torres, M. Elissondo, G. Pedreros, R. Aguilar, Á. Amigo, S. García, P. Forte, C. Bonadonna, Volcanic risk ranking and regional mapping of the Central volcanic Zone of the Andes, Nat. Hazards Earth Syst. Sci. 24 (2024) 4267–4291, https://doi.org/10.5194/nhess-24-4267-2024.
[13] C. Scaini, A. Felpeto, J. Martí, R. Carniel, A GIS-based methodology for the estimation of potential volcanic damage and its application to Tenerife Island, Spain, J. Volcanol. Geotherm. Res. 278–279 (2014) 40–58, https://doi.org/10.1016/j.jvolgeores.2014.04.005.
[14] C. Bonadonna, S. Biass, E. Calder, C. Frischknecht, C. Gregg, S. Jenkins, S. Loughlin, S. Menoni, S. Takarada, T. Wilson, 1st IAVCEI-GVM workshop: "from Volcanic Hazard to Risk Assessment", Geneva, 27-29 June 2018, https://vhub.org/resources/4498, 2018.
[15] S.F. Jenkins, R.J.S. Spence, J.F.B.D. Fonseca, R.U. Solidum, T.M. Wilson, Volcanic risk assessment: quantifying physical vulnerability in the built environment, J. Volcanol. Geotherm. Res. 276 (2014) 105–120, https://doi.org/10.1016/j.jvolgeores.2014.03.002.
[16] N.I. Deligne, S.F. Jenkins, E.S. Meredith, G.T. Williams, G.S. Leonard, C. Stewart, T.M. Wilson, S. Biass, D.M. Blake, R.J. Blong, C. Bonadonna, R.C. B, J.L. Hayes, D.M. Johnston, B.M. Kennedy, C.R. Magill, R. Spence, K.L. Wallace, J. Wardman, A.M. Weir, G. Wilson, G. Zuccaro, From anecdotes to quantification: advances in characterizing volcanic eruption impacts on the built environment, Bull. Volcanol. 84 (2022) 1–9, https://doi.org/10.1007/s00445-021-01506-8.
[17] J.L. Hayes, R.H. Fitzgerald, T.M. Wilson, A. Weir, J. Williams, G. Leonard, Linking hazard intensity to impact severity: mini review of vulnerability models for volcanic impact and risk assessment, Front. Earth Sci. 11 (2024) 1278283, https://doi.org/10.3389/feart.2023.1278283.
[18] B. Clarke, P. Tierz, E. Calder, G. Yirgu, Probabilistic volcanic hazard assessment for pyroclastic density currents from pumice cone eruptions at Aluto Volcano, Ethiopia, Front. Earth Sci. 8 (2020) 1–19, https://doi.org/10.3389/feart.2020.00348.
[19] N. Alcozer-Vargas, M.P. Reyes-Hardy, A. Esquivel, F. Aguilera, A GIS-based multi-hazard assessment at the San Pedro volcano, Central Andes, northern Chile, Front. Earth Sci. 10 (2022), https://doi.org/10.3389/feart.2022.897315.
[20] A. Aravena, A. Bevilacqua, A. Neri, P. Gabellini, D. Ferrés, D. Escobar, A. Aiuppa, R. Cioni, Scenario-based probabilistic hazard assessment for explosive events at the San Salvador volcanic complex, El Salvador, J. Volcanol. Geotherm. Res. 438 (2023), https://doi.org/10.1016/j.jvolgeores.2023.107809.
[21] E. Tennant, S.F. Jenkins, A. Winson, C. Widiwijayanti, H.D. Purnamasari, N. Kartadinata, W. Banggur, Probabilistic volcanic hazard assessment during quiescence: a scenario-based approach for Gede, West Java (Indonesia), Bull. Volcanol. 87 (2025) 126, https://doi.org/10.1007/s00445-025-01908-y.
[22] E. Aydar, P. Labazuy, C. Diker, Scenario-based hazard assessment of Mt Hasan Stratovolcano, Central Anatolia, Türkiye. Bull Volcanol 87 (2025) 37. https://doi.org/10.1007/s00445-025-01818-z.
[23] K.J. Beven, S. Almeida, W.P. Aspinall, P.D. Bates, S. Blazkova, E. Borgomeo, J. Freer, K. Goda, J.W. Hall, J.C. Phillips, M. Simpson, P.J. Smith, D.B. Stephenson, T. Wagener, M. Watson, K.L. Wilkins, Epistemic uncertainties and natural hazard risk assessment - part 1: a review of different natural hazard areas, Nat. Hazards Earth Syst. Sci. 18 (2018) 2741–2768, https://doi.org/10.5194/nhess-18-2741-2018.
[24] S. Biass, A. Todde, R. Cioni, M. Pistolesi, N. Geshi, C. Bonadonna, Potential impacts of tephra fallout from a large-scale explosive eruption at Sakurajima volcano, Japan, Bull. Volcanol. 79 (2017), https://doi.org/10.1007/s00445-017-1153-5.
[25] S.F. Jenkins, S. Biass, G.T. Williams, J.L. Hayes, E. Tennant, Q. Yang, V. Burgos, E.S. Meredith, G.A. Lerner, M. Syarifuddin, A. Verolino, Evaluating and ranking Southeast Asia's exposure to explosive volcanic hazards, Nat. Hazards Earth Syst. Sci. 22 (2022) 1233–1265, https://doi.org/10.5194/nhess-22-1233-2022.

[26] V. Pessina, F. Meroni, E. Varini, M. Longoni, L. Sandri, A. Garcia, A. Cappello, Towards a probabilistic risk analysis due to volcanic-hazards at Mount Etna, Ann. Geophys. 68 (2025), https://doi.org/10.4401/ag-9175.
[27] S. Biass, C. Bonadonna, L. Connor, C. Connor, TephraProb: a Matlab package for probabilistic hazard assessments of tephra fallout, J. Appl. Volcanol. 5 (2016), https://doi.org/10.1186/s13617-016-0050-5.
[28] D. Oramas-Dorta, G. Tirabassi, G. Franco, C. Magill, Design of parametric risk transfer solutions for volcanic eruptions: an application to Japanese volcanoes, Nat. Hazards Earth Syst. Sci. 21 (2021) 99–113, https://doi.org/10.5194/nhess-21-99-2021.
[29] R.J.S. Spence, I. Kelman, P.J. Baxter, G. Zuccaro, S. Petrazzuoli, Natural Hazards and Earth System Sciences residential building and occupant vulnerability to tephra fall, Nat. Hazards Earth Syst. Sci. 5 (2005) 477–494.
[30] G.T. Williams, S.F. Jenkins, S. Biass, H.E. Wibowo, A. Harijoko, Remotely assessing tephra fall building damage and vulnerability: Kelud Volcano, Indonesia, J. Appl. Volcanol. 9 (2020), https://doi.org/10.1186/s13617-020-00100-5.
[31] E.S. Meredith, S.F. Jenkins, J.L. Hayes, D.J.H. Chee, D. Lallemant, N.I. Deligne, S. Meletlidis, A. Felpeto. Developing Empirical Fragility Functions for Lava Flow Building Damage, 2025. https://doi.org/10.2139/ssrn.5324274.
[32] A. Hadianti, H. Ulinnuha, L.S. Heliani, A. Sarwadi, A. Kurniawan, J. Budisetiawan, L. Suhubawa, W. Suryanto, C. Pratama, B.W. Mutaqin, W. Nayati, Y. Bayumurti, R. Ilahi, S.Y. Widjonarko, Integrating multi-hazard risk analysis into spatial planning for small Island: study case of sangihe Island, in: IOP Conference Series: Earth and Environmental Science, IOP Publishing Ltd, 2021, https://doi.org/10.1088/1755-1315/799/1/012008.
[33] R.J. Blong, P. Grasso, S.F. Jenkins, C.R. Magill, T.M. Wilson, K. McMullan, J. Kandlbauer, Estimating building vulnerability to volcanic ash fall for insurance and other purposes, J. Appl. Volcanol. 6 (2017), https://doi.org/10.1186/s13617-017-0054-9.
[34] P. Bani, S. Kunrat, D.K. Syahbana, Insights into the recurrent energetic eruptions that drive Awu, among the deadliest volcanoes on Earth, Nat. Hazards Earth Syst. Sci. 20 (2020) 2119–2132, https://doi.org/10.5194/nhess-20-2119-2020.
[35] Global Volcanism Program, Volcanoes of the world, Awu (267040, https://doi.org/10.5479/si.GVP.VOTW5-2025.5.3, 2025.
[36] M.S. Bebbington, S.F. Jenkins, Intra-Eruption forecasting using analogue Volcano and eruption sets, J. Geophys. Res. Solid Earth 127 (2022), https://doi.org/10.1029/2022JB024343.
[37] J. Matahelumual, Gunung Awu. Volcanological Survey Indonesia, Bull Volc Surv Indones. 107 (1985) 1–51.
[38] S.K. Brown, S.F. Jenkins, R.S.J. Sparks, H. Odbert, M.R. Auker, Volcanic fatalities database: analysis of volcanic threat with distance and victim classification, J. Appl. Volcanol. 6 (2017), https://doi.org/10.1186/s13617-017-0067-4.
[39] Global Volcanism Program, Report on Awu (Indonesia), in: R. Wunderman (Ed.), Bull. Glob. Volcanism Netw. 29 (2004) 5, https://doi.org/10.5479/si.GVP.BGVN200405-267040. Smithsonian Institution.
[40] M. Cassidy, S.K. Ebmeier, C. Helo, S.F.L. Watt, C. Caudron, A. Odell, K. Spaans, P. Kristianto, H. Triastuty, H. Gunawan, J.M. Castro, Explosive eruptions with little warning: experimental petrology and Volcano monitoring observations from the 2014 eruption of Kelud, Indonesia, Geochem. Geophys. Geosystems 20 (2019) 4218–4247, https://doi.org/10.1029/2018GC008161.
[41] D. Blake, The 2014 eruption of Kelud Volcano, Indonesia : impacts on infrastructure, utilities, agriculture and health, GNS Science, Te Pū Ao (2015).
[42] World Population Review. https://worldpopulationreview.com/, 2024.
[43] Badan Pusat Statistik, Profil Ketenagakerjaan Kabupaten Kepulauan Sangihe, 2023.
[44] Badan Pusat Statistik, Statistik Daerah Kabupaten Kepuluan Sangihe, 2021.
[45] I. Khurun'in, J. Purnomo, Measuring Sustainable Livelihood in the Border Areas: the Case Study of Sangihe Island, vol. 1, North Sulawesi. JGF, 2021, pp. 117–130, https://doi.org/10.21776/ub.jgf.2021.001.02.2.
[46] R. Blong, A review of damage intensity scales, Nat. Hazards (2003).
[47] C. Bonadonna, J.C. Phillips, B.F. Houghton, Modeling tephra sedimentation from a Ruapehu weak plume eruption, J. Geophys. Res. Solid Earth 110 (2005) 1–22, https://doi.org/10.1029/2004JB003515.
[48] C.G. Newhall, S. Self, The volcanic explosivity index (VEI) an estimate of explosive magnitude for historical volcanism, J. Geophys. Res., Oceans 87 (1982) 1231–1238, https://doi.org/10.1029/JC087iC02p01231.
[49] S. Biass, C. Bonadonna, A quantitative uncertainty assessment of eruptive parameters derived from tephra deposits: the example of two large eruptions of Cotopaxi volcano, Ecuador, Bull. Volcanol. 73 (2011) 73–90, https://doi.org/10.1007/s00445-010-0404-5.
[50] C. Bonadonna, S. Biass, A. Costa, Physical characterization of explosive volcanic eruptions based on tephra deposits: propagation of uncertainties and sensitivity analysis, J. Volcanol. Geotherm. Res. 296 (2015) 80–100, https://doi.org/10.1016/j.jvolgeores.2015.03.009.
[51] H. Hersbach, B. Bell, P. Berrisford, S. Hirahara, A. Horányi, J. Muñoz-Sabater, J. Nicolas, C. Peubey, R. Radu, D. Schepers, A. Simmons, C. Soci, S. Abdalla, X. Abellan, G. Balsamo, P. Bechtold, G. Biavati, J. Bidlot, M. Bonavita, G.D. Chiara, P. Dahlgren, D. Dee, M. Diamantakis, R. Dragani, J. Flemming, R. Forbes, M. Fuentes, A. Geer, L. Haimberger, S. Healy, R.J. Hogan, E. Hólm, M. Janisková, S. Keeley, P. Laloyaux, P. Lopez, C. Lupu, G. Radnoti, P. de Rosnay, I. Rozum, F. Vamborg, S. Villaume, J.N. Thépaut, The ERA5 global reanalysis, Q. J. R. Meteorol. Soc. 146 (2020) 1999–2049, https://doi.org/10.1002/qj.3803.
[52] F. Maeno, S. Nakada, M. Yoshimoto, T. Shimano, N. Hokanishi, A. Zaennudin, M. Iguchi, A sequence of a plinian eruption preceded by dome destruction at Kelud volcano, Indonesia, on February 13, 2014, revealed from tephra fallout and pyroclastic density current deposits, J. Volcanol. Geotherm. Res. 382 (2019) 24–41, https://doi.org/10.1016/j.jvolgeores.2017.03.002.
[53] R.S.J. Sparks, Volcanic Plumes, Wiley, Chichester, 1997.
[54] R. Blong, Building damage in Rabaul, Papua New Guinea, 1994, Bull. Volcanol. 65 (2003) 43–54, https://doi.org/10.1007/s00445-002-0238-x.
[55] S. Osman, M. Thomas, J. Crummy, A. Sharp, S. Carver, Laboratory tests to understand tephra sliding behaviour on roofs, J Appl. Volcanol. 12 (2023) 11. https://doi.org/10.1186/s13617-023-00137-2.
[56] S.F. Jenkins, A. McSporran, T.M. Wilson, C. Stewart, G. Leonard, S. Cevuard, E. Garaebiti, Tephra fall impacts to buildings: the 2017–2018 Manaro Voui eruption, Vanuatu, Front. Earth Sci. 12 (2024), https://doi.org/10.3389/feart.2024.1392098.
[57] Badan Pusat Statistik, Sensus Penduduk, 2020. (https://www.bps.go.id/en).
[58] W. Sirko, S. Kashubin, M. Ritter, A. Annkah, Y.S.E. Bouchareb, Y. Dauphin, D. Keysers, M. Neumann, M. Cisse, J. Quinn, Continental-Scale building detection from high resolution satellite imagery. https://doi.org/10.48550/arXiv.2107.12283, 2021.
[59] G. Zuccaro, F. Cacace, R.J.S. Spence, P.J. Baxter, Impact of explosive eruption scenarios at Vesuvius, Journal of Volcanology and Geothermal Research 178 (2008) 416–453. https://doi.org/10.1016/j.jvolgeores.2008.01.005.
[60] S. Jenkins, R. Spence, Vulnerability Curves for Buildings and Agricultural Support Infrastructure (Technical Reports for EU FP7-ENV Project MIA-VITA, Contract Number: 211393), Cambridge Architectural Research, 2009.
[61] W. Marzocchi, L. Sandri, J. Selva, BET_EF: a probabilistic tool for long- and short-term eruption forecasting, Bull. Volcanol. 70 (2008) 623–632, https://doi.org/10.1007/s00445-007-0157-y.
[62] W. Marzocchi, L. Sandri, P. Gasparini, C. Newhall, E. Boschi, Quantifying probabilities of volcanic events: the example of volcanic hazard at Mount Vesuvius, J. Geophys. Res. Solid Earth 109 (2004) 1–18, https://doi.org/10.1029/2004JB003155.
[63] J.L. Hayes, S.F. Jenkins, M. Joffrain, Large uncertainties are pervasive in long-term frequency-magnitude relationships for volcanoes in Southeast Asia, Front. Earth Sci. 10 (2022), https://doi.org/10.3389/feart.2022.895756.
[64] Badan Pusat StatistikGross. Regional Domestic Product of Kepulauan Sangihe Regency by Industry 2020–2024, 2025.
[65] J.L. Hayes, T.M. Wilson, C. Magill, Tephra fall clean-up in urban environments, Journal of Volcanology and Geothermal Research 304 (2015) 359–377. https://doi.org/10.1016/j.jvolgeores.2015.09.014.
[66] E. Kriswati, S. Primulyana, S. Dirasutisna, Volcanic Hazard Map of Awu Volcano, North Sulawesi Province, Center for Volcanology and Geological Hazard Mitigation (CVGHM) (2016).
[67] United Nations Development Programme, PDNA – Post Disaster Needs Assessment: La Soufrière Volcanic Eruption, 2022.
[68] C. Yepes-Estrada, A. Calderon, C. Costa, H. Crowley, J. Dabbeek, M.C. Hoyos, L. Martins, N. Paul, A. Rao, V. Silva, Global building exposure model for earthquake risk assessment, Earthq. Spectra 39 (2023) 2212–2235, https://doi.org/10.1177/87552930231194048.

[69] E. Tennant, S.F. Jenkins, V. Miller, R. Robertson, B. Wen, S.-H. Yun, B. Taisne, Automating tephra fall building damage assessment using deep learning, Nat. Hazards Earth Syst. Sci. 24 (2024) 4585–4608, https://doi.org/10.5194/nhess-24-4585-2024.
[70] H. Craig, T. Wilson, C. Magill, C. Stewart, A.J. Wild, Agriculture and forestry impact assessment for tephra fall hazard: fragility function development and New Zealand scenario application, Volcanica 4 (2021) 345–367, https://doi.org/10.30909/vol.04.02.345367.
[71] S.F. Jenkins, T. Wilson, C. Magill, V. Miller, C. Stewart, R. Blong, W. Marzocchi, M. Boulton, C. Bonadonna, A. Costa, Volcanic ash fall hazard and risk, in: Global Volcanic Hazards and Risk, Cambridge University Press, 2015, pp. 173–221, https://doi.org/10.1017/CBO9781316276273.005.
[72] C. Magill, T. Wilson, T. Okada, Observations of tephra fall impacts from the 2011 Shinmoedake eruption, Japan, Earth Planets Space 65 (2013) 677–698, https://doi.org/10.5047/eps.2013.05.010.
[73] G. Wilson, T.M. Wilson, N.I. Deligne, J.W. Cole, Volcanic hazard impacts to critical infrastructure: a review, J. Volcanol. Geotherm. Res. 286 (2014) 148–182, https://doi.org/10.1016/j.jvolgeores.2014.08.030.
[74] O.D. Cardona, M. Ordaz, E. Reinoso, L.E. Yamin, CAPRA-Comprehensive Approach to Probabilistic Risk Assessment: International Initiative for Risk Management Effectiveness, 2012.
[75] C. Bonadonna, C. Frischknecht, S. Menoni, F. Romerio, C.E. Gregg, M. Rosi, S. Biass, A. Asgary, M. Pistolesi, D. Guobadia, A. Gattuso, A. Ricciardi, C. Cristiani, Integrating hazard, exposure, vulnerability and resilience for risk and emergency management in a volcanic context: the ADVISE model, J. Appl. Volcanol. 10 (2021), https://doi.org/10.1186/s13617-021-00108-5.
[76] R. Paulik, N. Horspool, R. Woods, N. Griffiths, T. Beale, C. Magill, A. Wild, B. Popovich, G. Walbran, R. Garlick, RiskScape: a flexible multi-hazard risk modelling engine, Nat. Hazards 119 (2023) 1073–1090, https://doi.org/10.1007/s11069-022-05593-4.
[77] C. Yepes Estrada, A. Rao, J.A. Ceballos, S. Jenkins, M. Pagani, V. Silva, L.G. Valencia Ramírez, C. Laverde, M. Mora, Scenario impact assessment for volcanoes using the OpenQuake engine, Ann. Geophys. 68 (2025) V110, https://doi.org/10.4401/ag-9172.
[78] G. Williams, Reducing uncertainty in building vulnerability and impact assessment for tephra hazards, in: Phd Thesis), Nanyang Technological University, Singapore, 2021.
[79] P. Aravena Pelizari, C. Geiß, P. Aguirre, H. Santa María, Y. Merino Peña, H. Taubenböck, Automated building characterization for seismic risk assessment using street-level imagery and deep learning, ISPRS J. Photogramm. Remote Sens. 180 (2021) 370–386, https://doi.org/10.1016/j.isprsjprs.2021.07.004.
[80] S. Meng, M.H. Soleimani-Babakamali, E. Taciroglu, Automatic roof type classification through machine learning for regional wind risk assessment. https://doi.org/10.48550/arXiv.2305.17315, 2023.
[81] F. Gouveia, V. Silva, J. Lopes, R.S. Moreira, J.M. Torres, M. Simas Guerreiro, Automated identification of building features with deep learning for risk analysis, Discov. Appl. Sci. 6 (2024), https://doi.org/10.1007/s42452-024-06070-2.
[82] R. Spence, A. Pomonis, P. Baxter, A. Coburn, M. White, M. Dayrit, Field Epidemiology Training Program Team, Building damage caused by the Mount Pinatubo eruption of June 15, 1991, in: Fire and Mud: Eruptions and Lahars of Mount Pinatubo, Philippines, 1996.
[83] Pesaresi, M., 2023. GHS-BUILT-S R2023A - GHS built-up surface grid, derived from Sentinel2 composite and Landsat, multitemporal (1975-2030).doi.org/10.2905/9F06F36F-4B11-47EC-ABB0-4F8B7B1D72EA.
[84] J.A. de Bruijn, J.E. Daniell, A. Pomonis, R. Gunasekera, J. Macabuag, M.C. de Ruiter, S.J. Koopman, N. Bloemendaal, H. de Moel, J.C.J.H. Aerts, Using rapid damage observations for Bayesian updating of hurricane vulnerability functions: a case study of Hurricane Dorian using social media, Int. J. Disaster Risk Reduct. 72 (2022), https://doi.org/10.1016/j.ijdrr.2022.102839.
[85] G.G. Tekeste, A.A. Correia, A.G. Costa, Bayesian updating of seismic fragility curves through experimental tests, Bull Earthquake Eng 21 (2022) 1943–1976, https://doi.org/10.21203/rs.3.rs-1415713/v2.
[86] A. Singhal, A.S. Kiremidjian, Bayesian updating of fragilities with application to RC frames, J. Struct. Eng. 124 (1998) 922–929, https://doi.org/10.1061/(ASCE)0733-9445(1998)124:8(922.